國立交通大學

電機學院　電信學程

碩 士 論 文

全球衛星導航系統信號之數位載波及亂碼追蹤

Digital Carrier and Code Tracking for Global Navigation Satellite System

研 究 生：楊儒木

指導教授：蘇育德　教授

中 華 民 國 九 十 八 年 一 月

全球衛星導航系統信號之數位載波及亂碼追蹤

Digital Carrier and Code Tracking for Global Navigation Satellite System

研 究 生：楊儒木　　Student：Ru-Muh Yang

指導教授：蘇育德 博士　　Advisor：Dr. Yu T. Su

國 立 交 通 大 學

電機學院　電信學程

碩 士 論 文

A Thesis

Submitted to College of Electrical and Computer Engineering

National Chiao Tung University

in partial Fulfillment of the Requirements

for the Degree of

Master of Science

in

Communication Engineering

January 2009

Hsinchu, Taiwan, Republic of China

中華民國九十八年一月

全球衛星導航系統信號
之數位載波及亂碼追蹤

學生：楊儒木　　指導教授：蘇育德 博士

國立交通大學　　電機學院　　電信學程碩士班

摘　　要

以軟體方式實現的 GPS 接收機，為了降低計算負擔與儲存空間，並達成即時性的需求，往往會採用很少位元的類比數位轉換器(ADC)，甚至僅採用單一位元的類比數位轉換器(ADC)。然而伴隨此少位元 ADC 而來的是接收性能的損失，本文探討少位元 ADC 因素所導致的性能損失，並提出一因應的載波相位補償結構做法，稱為後相關器相位補償(PCPC)結構，以改善此性能損失。

另外，在載波相位鑑別器方面，一般最常使用的是正切的反函數(arctangent)，主要是基於 arctangent 對於類比訊號可獲致最大訊雜比(SNR)。然而在採用低位元 ADC 的情況下，其量化誤差(quantization error)也是不可忽略的因素。針對此，本文提出一新型的載波相位鑑別器，稱為 NB-DPD，此鑑別器經模擬分析與實驗驗證：在高訊雜比的環境下，其性能優於 arctangent；而在低訊雜比的環境下，則其性能與 arctangent 是不相上下的，但在計算負擔上則優於 arctangent。本文並推導與分析此鑑別器的統計特性。

由於 NB-DPD 具備高效率與高精度的特性，且在數位技術不斷發展的趨勢中，是 GPS 接收機非常適用的載波相位鑑別器。

Digital Carrier and Code Tracking for Global Navigation Satellite System

Student: Ru-Muh Yang Advisor: Dr. Yu T. Su

Degree Program of Electrical and Computer Engineering
National Chiao Tung University

ABSTRACT

When implementing a software-GPS-receiver (SGR), few bits analog-to-digital converter (ADC) are usually selected to reduce the required computation and storage. In this thesis, the performance degradation induced by few bits ADC is discussed and an improved structure called post-correlator phase compensation (PCPC) is proposed. The significant feature of the PCPC structure is the improvement of correlator output magnitude because it prevents the quantization effect on carrier phase ambiguity. The improvement becomes more critical when one-bit ADC is used.

On the other hand, in a SGR, the carrier synchronization typically adopts arctangent or its approximations as the phase discriminator because it maximizes SNR for analog signal cases. However, for few-bits ADC, this method greatly reduces the accuracy of phase estimate because of the significant quantization error. In this thesis, a novel phase discriminator, called NB-DPD, is proposed for one-bit ADC SGR. The statistical properties of the NB-DPD estimator are provided. The analytical results are verified by computer simulation. In addition, the NB-DPD is equivalent to DPD[1] in noiseless case and thus inherits high accuracy properties of DPD in high SNR cases. The NB-DPD performs generally better than the DPD in noisy cases. The lower the SNR is, the greater the improvement. Moreover, the NB-DPD works almost as well as arctangent-phase discriminator (APD) in low SNR environments and thus can be

applied to GNSS receivers.

Finally, the NB-DPD is implemented in a one-bit software-defined GPS receiver using PCPC structure. The experimental results demonstrate the feasibility of the proposed scheme.

誌　　謝

本論文得以完成，承蒙恩師蘇育德教授所給予的悉心指導，使我克服研究中所遭遇的困難，並得到深度的學習，謹表示誠摯的感謝。同時也感謝口試委員呂忠津教授、高銘盛教授與張介福博士提供寶貴的意見與指導，使論文更加完整，實衷心感激。

另外，特別感謝同事張介福博士，幫助我解決許多研究上的困難，使我能順利完成本論文。

最後，我要對我的家人表示最大的謝意。由於是在工作中的再進修，不免忽略了一些對家人應有的關懷與對家庭應盡的責任，對於家人的諒解與支持，我衷心的感激。

Contents

List of Figures

1. Introduction

This thesis consists of six chapters. Chapter 2 introduces the modern Global Navigation Satellite Systems (GNSS) including GPS, GLONASS, Galileo and Beidou-2 systems. Our work focuses on Global Position System (GPS) and the associated receiver and signals are introduced. In Chapter 3, the first problem we are going to address: the carrier phase ambiguity induced by few-bits quantization is discussed. An improved carrier tracking structure called post-correlator phase compensation (PCPC) structure is proposed for real-time software GPS receiver with one-bit analog-to-digital converter (ADC). We also discuss a number of implementation issues of the PCPC structure. Next, in Chapter 4, we propose a novel phase discriminator called NB-DPD, which is modified from digital phase discriminator (DPD)[1] and provides a better performance in noisy environments. The probability-density-function (pdf), mean and variance of the NB-DPD estimator are also derived. Next, Chapter 5 provides the simulation results of the NB-DPD estimator and the experimental results of the tracking loop for GPS signal receiving. Finally, Chapter 6 concludes the work.

2. Global Navigation Satellite Systems (GNSS)

We summarize the modern GNSS systems as follow[2] [3] [4] [6]

2.1 Current in-operation GNSS systems

Global Navigation Satellite System (GNSS) is a satellite system that is used to pinpoint the geographic location of a user's receiver anywhere in the world. All the GNSS systems employ a constellation of orbiting satellites working in conjunction with a network of ground stations.

Two GNSS systems currently in operation are: the United States' Global Positioning System (GPS) and the Russian Federation's GLONASS. A third, Europe's Galileo, is slated to reach full operational capacity in 2013. Besides, the China BeiDou-1 is a regional navigation satellite system currently in operation, China plan to upgrade BeiDou-1 to a global coverage GNSS system via COMPASS/BeiDou-2.

The main parameters of the GNSS system are shown in Figure 2.1-1, and the spectrum arrangement for the GPS, Galileo and GLONASS is shown in Figure 2.1-2.

	GPS	GLONASS	Compass/BeiDou-2	Galileo
Developer	USA	Russia	China	EU
Constellation (Satellite number)	24	24 @ 1995 18 @ 2007 24 @ 2011[1]	30 MEO 5 GEO[3]	30[5]
Orbit	Medium Earth Orbit 19,222km (altitude) Circular	Medium Earth Orbit 19,100 km (altitude) Circular	Medium Earth Orbit 21,150 km (altitude) Circular	Medium Earth Orbit 23,222 km (altitude) Circular
Orbit plane	6 (60° apart)	3 (120° apart)	(N/A)	3 (120° apart)
Orbit period	11 hr 58 min	11 hr 15 min	(N/A)	10 days/ 17 orbits (14 hr 7 min)
Inclination	55°	64.8°	55.5°	56°
Coverage	Global	Global	BeiDou-2: Global BeiDou-1: China and the surrounding area, 5°N~55°N, 70°E~140°E	Global
Frequency	L1:1,575.42MHz L2:1,227.6MHz L5:1,176.45MHz	1,246~1,257MHz 1,602~1,616MHz[2]	Uplink: (L-band) 1,610~1,626.5MHz Downlink: (S-band) 2,483.5~2,500MHz SBAS: [4] L1, L2	E2-L1-E1: 1,559~1,592MHz E6:1,260~1,300MHz E5:1,164~1,215MHz
Bring into use	1993	1993	BeiDou-1: 2003 BeiDou-2: 2008	2013[6]
Note	1. GLONASS constellation will consist of 21 active satellites plus 3 active on-orbit spares. 2. GLONASS employs FDMA, i.e., each GLONASS satellite transmits the same PRN code pair on different frequency. 3. GEO satellites of BeiDou-1 project are located at 80°E, 140°E, and 110°E . 4. BeiDou SBAS payload is likely used to augment both GPS and GLONASS. 5. GALILEO comprise 27 operational satellites plus 3 spare satellites. 6. GALILEO is expected to be full operational in 2013.			

Figure 2.1-1 Main parameters of the existing GNSS systems

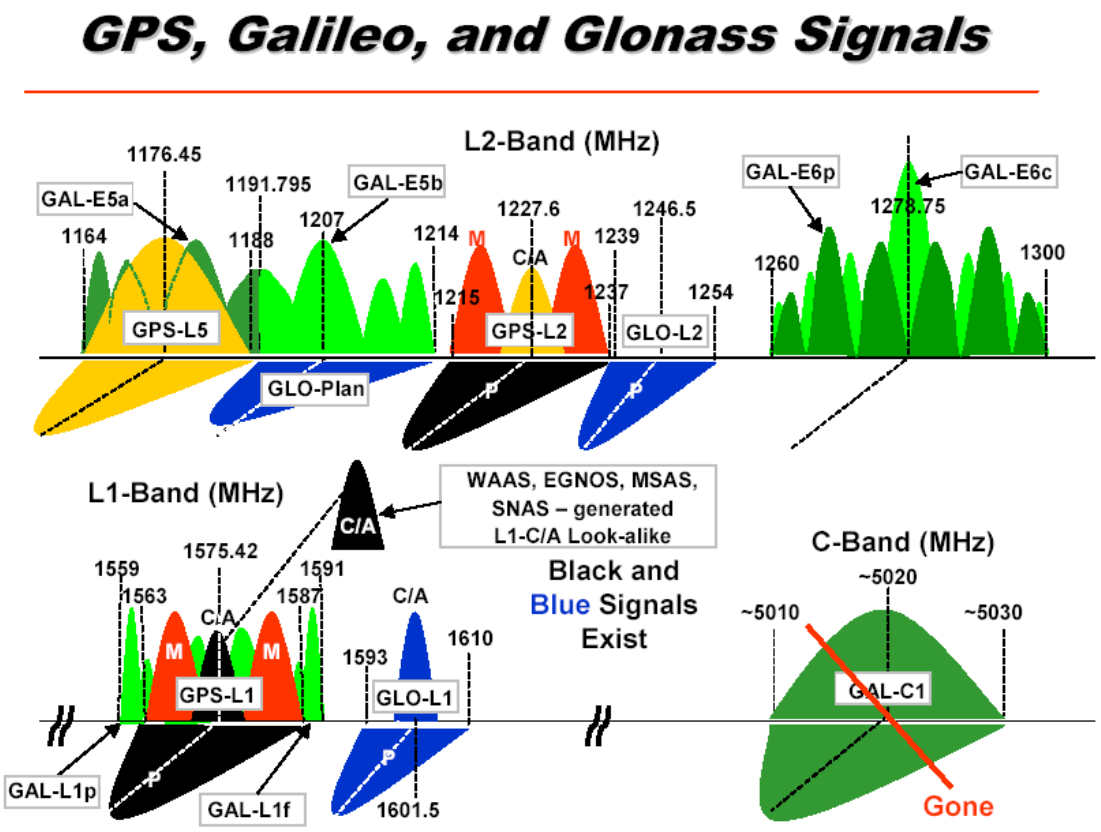

Figure 2.1-2 GNSS spectrum arrangement including GPS, GLONASS, and Galileo

2.2 Global positioning system (GPS) signals

2.2.1 Legacy GPS signals

GPS reached full operational capability in early 1995, the 24 satellites originally broadcast ranging codes and navigation data on two frequencies using CDMA technique; that is, there are only two frequencies in use by the system, called L1 (1.575.42 MHz) and L2 (1,227.6 MHz). Each satellite transmits on these frequencies, but with different ranging codes than those employed by other satellites. The Gold code is selected because of its low cross-correlation properties. Each satellite generates a short code referred to as the coarse/acquisition (C/A) code and a long code denoted as the precision or P(Y) code. The navigation data provides the means for the receiver

to determine the location of the satellite at the time of signal transmission, whereas the ranging code enables the user's receiver to determine the satellite (i.e., propagation) time of the signal and thereby determine the satellite-to-user range.

The L1 frequency is modulated by two PRN codes (plus the navigation message data), the C/A code, and the P code. The L2 frequency is modulated by only one PRN code at a time. The C/A code has a chipping rate of 1.023 Mchips/s and the P code has a chipping rate of 10.23 Mchips/s. The P code is modulated in phase quadrature with the C/A code on L1. The P code signal is 3-dB low relative to the C/A code on L1. The legacy L1 signals can be represented as follow.

$$L_1(t) = A[P(t) \oplus D(t)]\cos(\omega t) + \sqrt{2}A[C(t) \oplus D(t)]\sin(\omega t) \qquad (2.2.1\text{-}1)$$

where, A denotes amplitude, $P(t)$ denotes P code, $D(t)$ denotes navigation data, and C denotes C/A code.

2.2.2 Modernized GPS signals[3]

In January 1999, the U.S. government announced a new GPS modernization initiative that called for the addition of two civil signals to be added to new GPS satellites. These signals are denoted as L2C and L5. The L2C signal is at the L2 frequency; the L5 signal resides in ARNS band at 1,176.45 MHz. These additional signals will provide civil, commercial and scientific users the ability to correct for ionospheric delays by making dual frequency measurement, thereby significantly increasing civil user accuracy. The additional signals also increase the receiver's robustness to interference.

1). L2 civil signal

The L2 civil (L2C) signal has a similar power spectrum (i.e., 2.046 MHz null-to-null bandwidth) to the C/A code. However, the L2C uses two different PRN codes per satellite. The first PRN code is referred to as the civil moderate (CM) code which employs a sequence that repeats every 10,230 chips. The second code, the civil long (CL) code, is extremely long with a length of 767,250 chips. These two codes are generated each at a 511.5 kchip/s rate. The CM code is modulated by a 25-bps navigation data stream. The baseband L2C signal is formed by the chip-by-chip multiplexing of the CM (with data) and the CL codes. Hence the L2C signal has an overall chip rate of 2 × 511.5 kchip/s rate = 1.023 Mchip/s, which account for its similar power spectrum to the C/A code.

2). L5 signal

L5 signal uses QPSK modulation to combine an in-phase signal component (I5) and a quadraphase signal component (Q5). Different PRN codes with same length-10,230 are used for I5 and Q5. The I channel is the data channel and the Q channel is the pilot (no data) channel. I5 is modulated by 50-bps navigation data. A 10.23 MHz chipping rate is employed for both the I5 and Q5 PRN codes resulting a 1-ms code repetition period.

3). M code

During the mid to late 1990s, a new military signal called M code was developed for the military users. This signal will be transmitted on both L1 and L2 and is spectrally separated from the GPS civil signals in those bands. The spectral separation permits the use of non-interfering higher power M code modes that increase resistance to interference. The M code is intended to eventually replace the P(Y) code.
The new M code employs binary-offset-carrier (BOC) modulation. Specifically, M code is a BOC (10, 5) signal. The first parameter denotes the frequency of a square-wave subcarrier, which is 10 × 1.023 MHz, and the second parameter denotes the M code generator code chipping rate, which is 5 × 1.023 Mchip/s.

2.3 GPS receiver

1) Receiver structure[4]

The structure of a typical GPS receiver is shown in Figure 2.3-1. The signal transmitted from the GPS satellites are received from the antenna. Through the RF chain the input signal is amplified to proper amplitude and the frequency is converted to a desired IF frequency. An analog-to-digital converter (ADC) is used to digitize the output signal. The antenna, RF chain, and ADC are the necessary hardware used in the receiver.

After the signal is digitized, a software approach can be taken to perform the subsequent processes. The Acquisition is to find the signal of a certain satellite. The Tracking program is used to find the phase transition of the navigation data. In a conventional receiver, the Acquisition and Tracking are performed by hardware. From the navigation data phase transition, the subframes and navigation data can thus be obtained. Ephemeris data and pseudoranges can be obtained from the navigation data. The ephemeris data are used to obtain the satellite position. Finally, the user position can be calculated from the satellite positions and the pseudoranges.

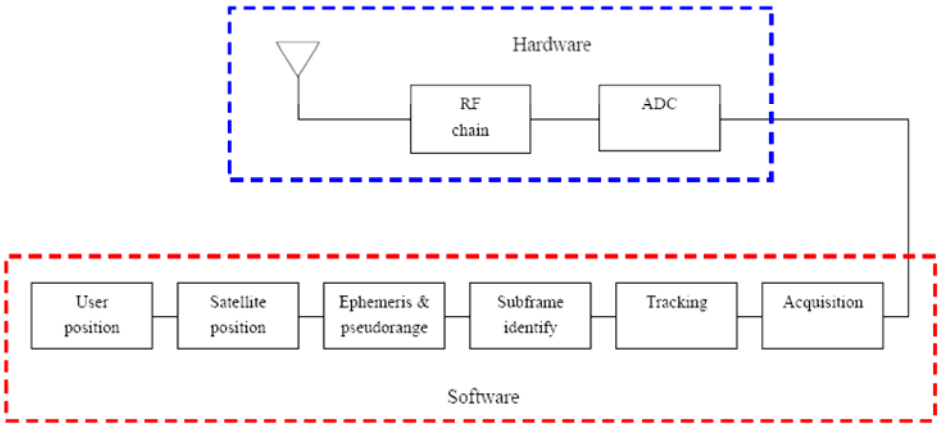

Figure 2.3-1 A fundamental GPS receiver

2) Signal-to-Noise Ratio (SNR) [10]

The L1 C/A code signal is transmitted at a minimal level of 478.63W (26.8 dBW) effective isotropic radiated power (EIRP). The free-space loss factor (FSLF) is given by $FSLF = (\frac{\lambda}{4\pi R})^2$

where, R is the distance between GPS satellite and the receiver, λ is the wavelength. Using $R = 2\times10^7$ and $\lambda = 0.19m$ at L1 frequency, the FSLF is about -182.4 dB. An additional atmospheric loss factor (ALF) is about 2 dB, and if the receiving antenna is assumed to be isotropic, then the received signal power is EIRP-FSLF-ALF=26.8-182.4-2=-157.6 dBW. Since a typical GPS antenna with right-hand circular polarization and a hemispherical pattern has about 3 dB of gain, the result of minimum received signal power is -157.6+3= -154.6 dBW.

The noise power in the first RF amplifier stage of the receiver front end is given by $N = kT_eB$, where, $k = 1.3806\times10^{-23}\ J/K$, B is the bandwidth in Hz, and T_e is the effective noise temperature in degree Kelvin. A typical effective noise temperature for a GPS receiver is 513 K, resulting in a noise power of about -138.5 dBW in a 2MHz bandwidth. As about 90% of the C/A-code power lies in a 2-MHz bandwidth, so there is only about 0.5 dB loss in signal power. Consequently, the SNR in a 2MHz bandwidth is (-154.6-0.5)-(-138.5)= -16.6 dB.

Since the SNR is far below 0 dB, the signal is buried in noise. In this thesis, we will focus the analysis on low SNR environments as of around -20 dB.

3) Software-GPS Receiver (SGR)

Software receivers have drawn more and more attention because of their flexibility to demodulate a number of distinct RF transmissions and the removal of several analog components at RF band. When implementing a real-time SGR (Software-GPS Receiver), owing to the correspondingly high sampling rate, 1 or 2-bits quantization is usually selected in order to reduce computation and storage load. However, few bits quantization may induce significant degradation[2] [5]. An improved tracking structure called post-correlator phase compensation (PCPC) structure and a novel carrier phase discriminator called noise-balanced digital phase discriminator (NB-DPD) are proposed in the thesis.

3. Tracking Loop in One-bit Software-GPS Receiver (SGR)

3.1 Conventional tracking loop

The tracking of a GPS receiver consists of the code tracking and carrier tracking loops, which locks onto and tracks the PRN code and carrier of the GPS satellite signal respectively. A typical tracking structure is shown in Fig 3.1-1.

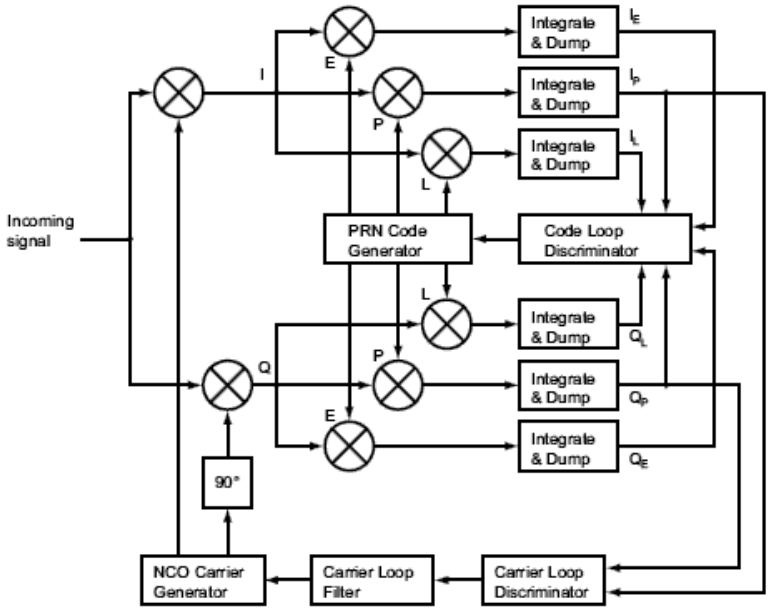

Fig 3.1-1 combined code and carrier tracking loop

For the code tracking, the delay-lock-loop (DLL) is used to make the receiver-generated code line up with incoming code precisely. In Fig 3.1-1, three different replica code phases, early, prompt, and late, for both I- and Q-channels are correlated simultaneously with the same incoming signal. The early and late codes respectively lead and lag the prompt code by less than 0.5 code chips and always maintain these relative positions.[10] In normal operation the prompt code is aligned with the code of the incoming signal so that the squared magnitude $I_P^2 + Q_P^2$ of the prompt correlator output is at the peak of the cross-correlation function, and the output magnitude of the early and late correlators have smaller but equal values on each side of the peak. Fig 3.1-2 shows the early, prompt, and late envelopes as the phases of the replica code signals are advanced/ aligned with respect to the incoming signals.

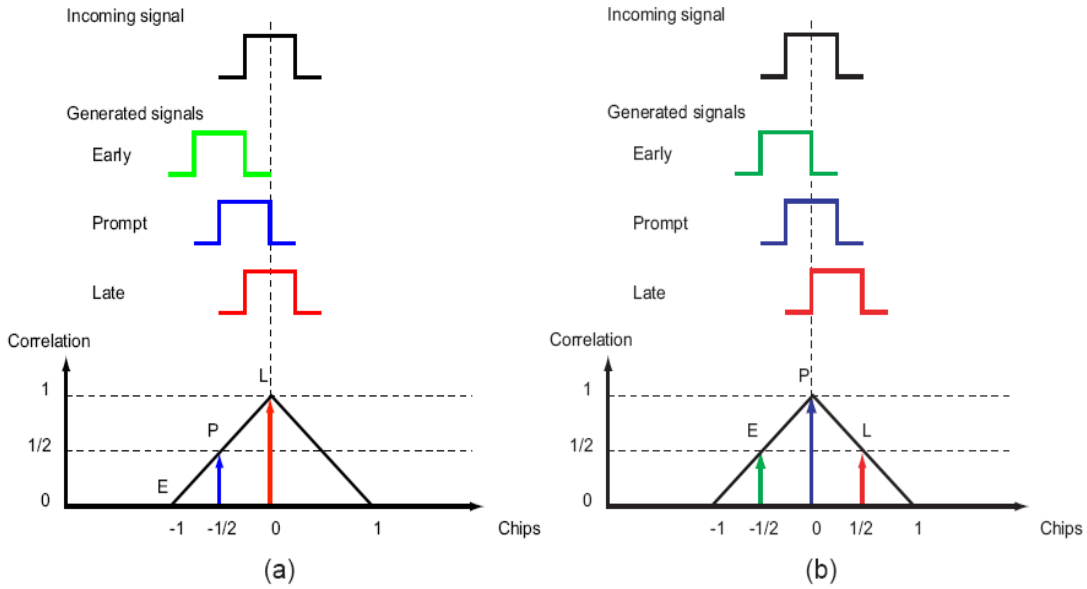

Fig 3.1-2 Code correlation phases: (a) replica code 1/2-chip early, (b) replica code aligned

In Fig 3.1-1, the carrier tracking loop consists of the prompt correlator, carrier loop discriminator, carrier loop filter, and numerical-control oscillator (NCO). The discriminator is used to estimate carrier phase error and the loop filter is to reduce noise. The loop filter order and noise bandwidth also determine the filter's response to signal dynamics. In accordance to the estimated phase error, NCO aligns the phase and frequency of the local carrier to synchronize the incoming signal.

3.2 Post-correlator phase compensation (PCPC) tracking structure for 1-bit SGR

3.2.1 Problem description

Firstly, let's consider the quantization effect on the conventional carrier tracking loop. For SGR, we have pre-established sine table and cosine tables given by

$$LO_I(n) = \cos(2\pi fnT_s)$$
$$LO_Q(n) = \sin(2\pi fnT_s)$$

where f is the local carrier frequency and T_s is the sampling period. The tables usually use very few bits per sample in order to save computation and storage. For 1-bit ADC SGR, the received data $S(n)$ and the local carrier are quantized as two values given by

$$LO_I(n) = \mathrm{sgn}\left(\cos(2\pi fnT_s)\right)$$
$$LO_Q(n) = \mathrm{sgn}\left(\sin(2\pi fnT_s)\right),$$

where sgn(x) denotes the polarity function of x. Hence for a given n, the local carrier has four possibilities on I-Q plane as shown in Figure 3.2-1(a). In traditional carrier tracking loop as shown in Figure 3.2-2, the phase is estimated by the discriminator, and the carrier generated by numerical-control oscillator (NCO) is then phase compensated accordingly as follows.

$$\begin{aligned} LO'_I(n) &= \cos(2\pi fnT_s + \hat{\theta}) \\ &\approx \cos\hat{\theta}\cdot\mathrm{sgn}(\cos(2\pi fnT_s)) - \sin\hat{\theta}\cdot\mathrm{sgn}(\sin(2\pi fnT_s)) \\ LO'_Q(n) &= \sin(2\pi fnT_s + \hat{\theta}) \\ &\approx \sin\hat{\theta}\cdot\mathrm{sgn}(\cos(2\pi fnT_s)) + \cos\hat{\theta}\cdot\mathrm{sgn}(\sin(2\pi fnT_s)) \end{aligned}$$

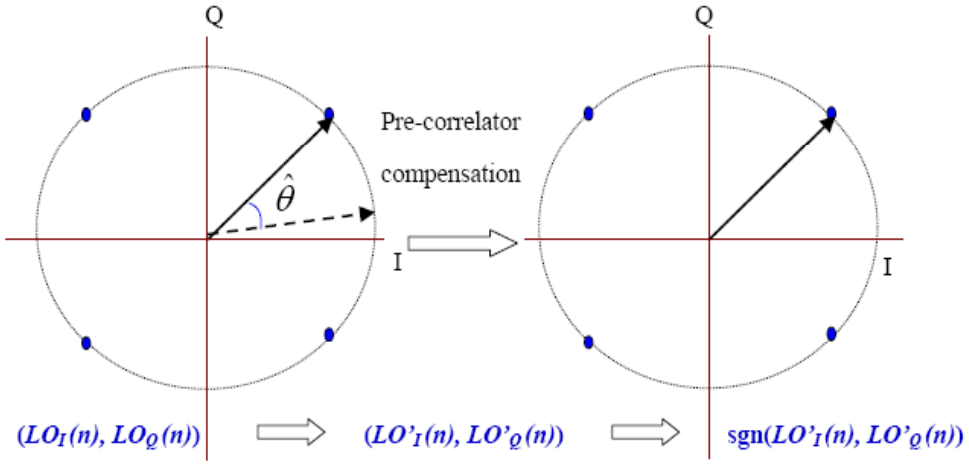

(a) (b)

Figure 3.2-1 Schematic plot for pre-correlator phase compensation tracking loop

In order to compute efficiently, the multiplication between $S(n)$ and local carrier is achieved by bitwise processing such as XOR operation. Hence the compensated NCO signals, $LO'_I(n)$ and $LO'_Q(n)$, are quantized as follows.

$$LO_I''(n) = \mathrm{sgn}(LO_I'(n)) = \mathrm{sgn}(\cos\hat{\theta}\,\mathrm{sgn}(\cos(2\pi fnT_s)) - \sin\hat{\theta}\,\mathrm{sgn}(\sin(2\pi fnT_s)))$$
$$LO_Q''(n) = \mathrm{sgn}(LO_Q'(n)) = \mathrm{sgn}(\sin\hat{\theta}\,\mathrm{sgn}(\cos(2\pi fnT_s)) + \cos\hat{\theta}\,\mathrm{sgn}(\sin(2\pi fnT_s)))$$

The signal constellation on I-Q plane after phase compensation is shown in Figure 3.2-1(b). From Figure 3.2-1, the phase ambiguity of local carrier is π/2 (±π/4) because we only have 4 possibilities on I-Q plane. Similarly, as we have m-bit ADC carrier table for pre-correlator phase compensation structure in SGR, the resultant phase ambiguity is given by

$$\theta_{amb} = \frac{\pi}{2^m}\left(\pm\frac{\pi}{2^{m+1}}\right)$$

Hence the degradation on the magnitude of in-phase correlator output is given by

$$Degradation = 10\log_{10}\left(\cos\frac{\theta_{amb}}{2}\right)(dB)$$

The fewer bits we use, the more degradation we suffer because of the quantization effect.

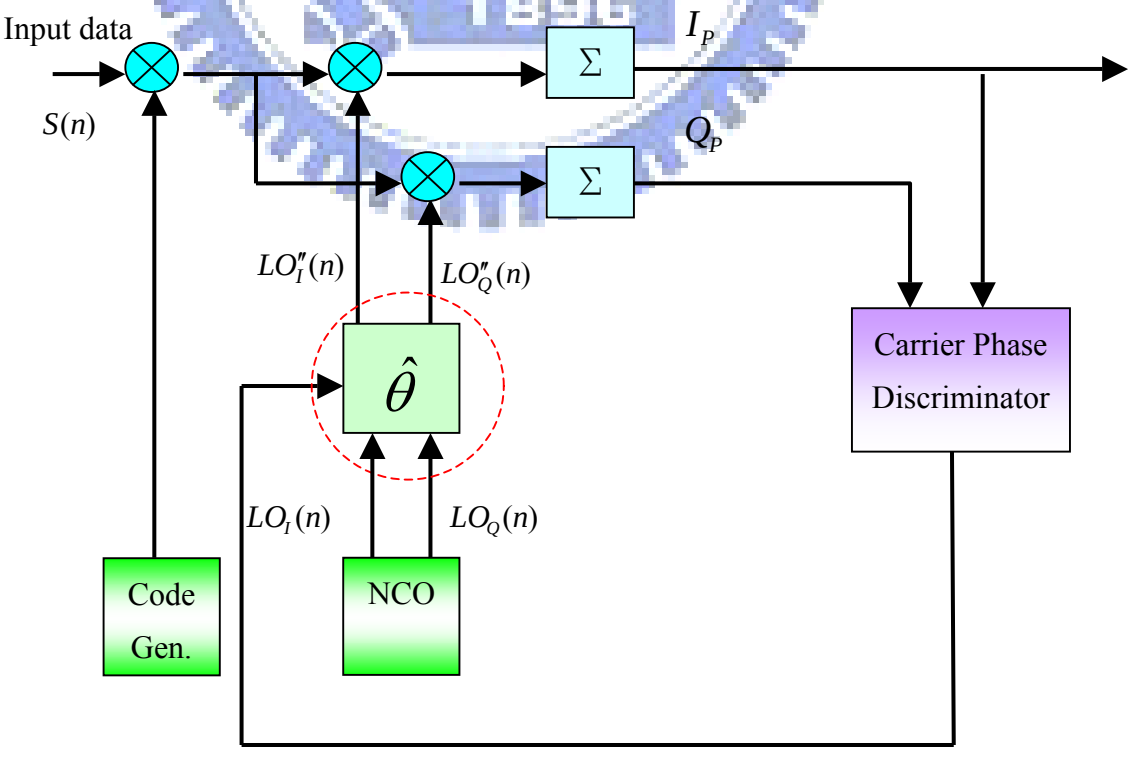

Figure 3.2-2 Simplified pre-correlator phase compensation tracking loop

3.2.2 The Proposed PCPC structure

In order to resolve the phase ambiguity problem induced by few-bits quantization, we propose a structure as shown in Figure 3.2-3, where Figure 3.2-3(a) is a simplified version and the Figure 3.2-3(b) is a complete system structure. Compared with the traditional one as in Figure 3.2-2, the proposed structure compensates the correlator output of I-channel with the estimated carrier phase after correlators in order to avoid significant phase ambiguity induced by few bits quantization.

Hence the proposed structure is called post-correlator phase compensation (PCPC) structure and the phase can be compensated accurately as shown in Figure 3.2-4.

In order to investigate the features of PCPC structure, we categorize components after phase discriminator into three groups as follows.

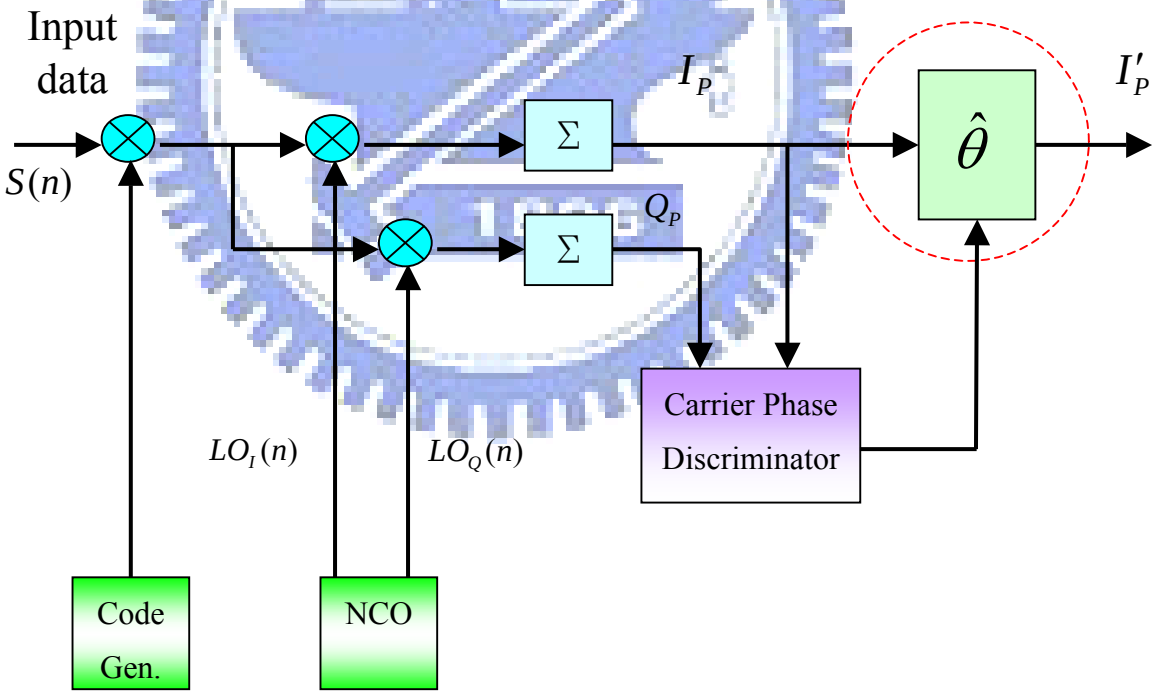

Figure 3.2-3(a) Simplified post-correlator phase compensation (PCPC) tracking loop

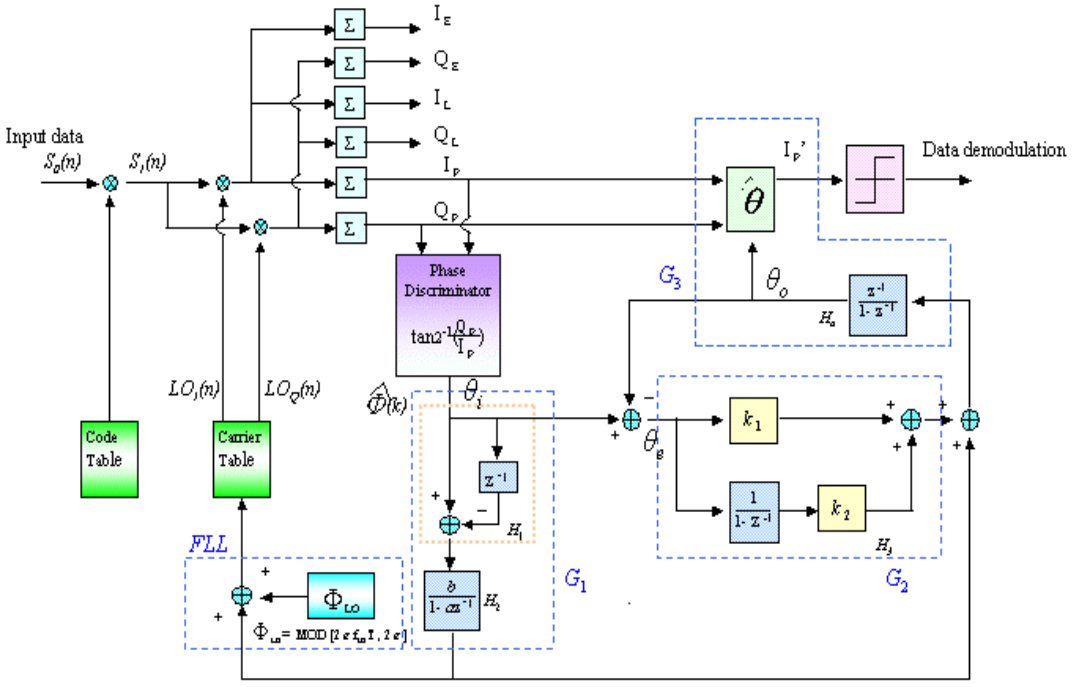

Figure 3.2-3(b) Implemented post-correlator phase compensation (PCPC) tracking loop

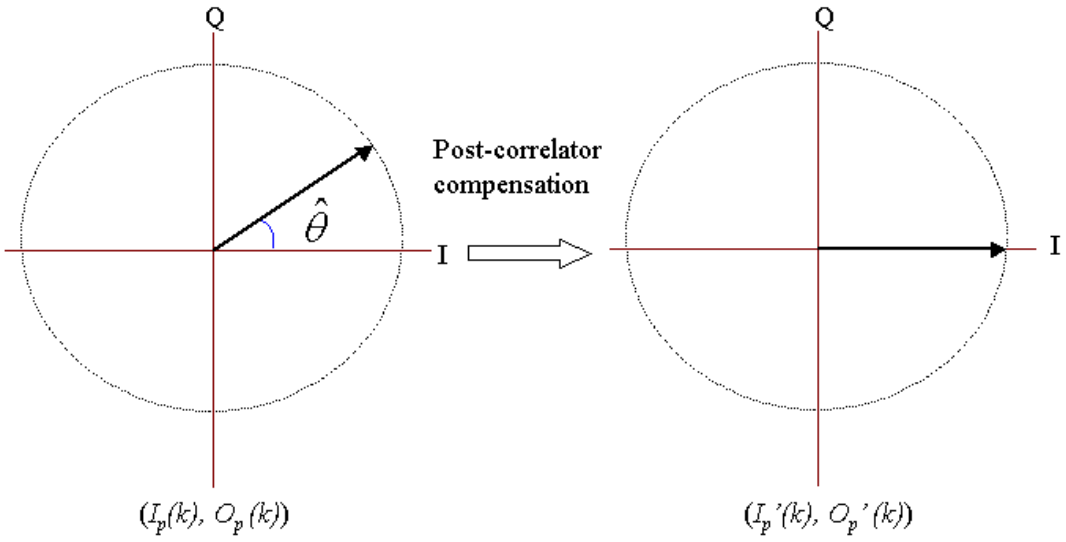

Figure 3.2-4 Schematic plot for post-correlator phase compensation tracking loop

Group G1 (phase-rotation part): The phase rotation in every observation interval is due to frequency offset and the beginning phase offset of pre-established carrier table. G1 includes a high-pass-filter H1 and a low-pass-filter H2. The phase-rotation component of input signal is extracted through H1. The implemented frequency response of H1 is given by

$$H_1(z) = 1 - z^{-1}. \tag{3.2-1}$$

Then H2 suppresses disturbances such as noise. The frequency response of H2 is given by

$$H_2(z) = \frac{b}{1 - az^{-1}} \tag{3.2-2}$$

The output of H2 can be used further to estimate frequency variation such as Doppler shift or carrier frequency bias, and hence the frequency-lock-loop (FLL) is achieved. Note that phase offset induced by carrier table as shown in Figure 3.2-5 must be compensated as well so that an accurate frequency estimate is obtained.

Group G2 (loop filter part): G2 acts as the loop filter and handles the phase-error component of the output of phase discriminator. The implemented frequency response of a 2nd order loop filter is given by

$$H_3(z) = k_1 + \frac{k_2}{1 - z^{-1}}. \tag{3.2-3}$$

Group G3 (phase estimate): G3 combines the phase-rotation part and the phase-error component. The estimated phase is then obtained. The implemented frequency response of the filter H4 is given by

$$H_4(z) = \frac{z^{-1}}{1 - z^{-1}} \tag{3.2-4}$$

Finally, the in-phase output I_P is compensated as follows:

$$I'_P = [\cos(\hat{\theta}_O) \quad \sin(\hat{\theta}_O)] \begin{bmatrix} I_P \\ Q_P \end{bmatrix} \tag{3.2-5}$$

3.2.3 Analysis

The analysis of analog PLL has been well established for decades [7][8]. In the following, we analyze the proposed carrier tracking structure based on digital approach, which is more appropriate for SGR.

Suppose the received data is given by

$$S_0[n] = D[n]C[n]\cos(2\pi f_c nT_s + \phi[n]) + u''[n],$$

where, $D[n]$ is navigation data, $C[n]$ is PRN code and $u''[n]$ is additive white Gaussian noise. Suppose that local PRN code $\hat{C}[n]$ perfectly matches $C[n]$. Then

$$S_1[n] = D[n]\cos(2\pi f_c nT_s + \phi[n]) + u'[n],$$

where

$$u'[n] = u''[n]\hat{C}[n]$$
$$= u'_I[n]\cos(2\pi fnT_s + \phi[n]) + u'_Q[n]\sin(2\pi fnT_s + \phi[n]),$$

and $u'_I[n]$ and $u'_Q[n]$ are real part and imaginary part of $u'[n]$, respectively. Suppose the local carrier are given by

$$LO_I[n] = \cos(2\pi fnT_s),$$
$$LO_Q[n] = \sin(2\pi fnT_s).$$

As we use pre-established carrier table which contains the data for n=0,1,2…N-1, i. e., the beginning phase of data is always zero. However, the initial phase of each received data may be not zero and change from interval to interval. Hence the true local carrier should incorporate a correct offset given by

$$LO_I[n] = \cos(2\pi fnT_s - k\Phi_{LO}),$$

$$LO_Q[n] = \sin(2\pi fnT_s - k\Phi_{LO}),$$

where $\Phi_{LO} = 2\pi fT \bmod 2\pi$, T is the observation period, and $k = \left\lfloor \frac{n}{N} \right\rfloor$, where $\lfloor x \rfloor$ is

a function rounding x to the greatest smaller integer, and N is the total samples within T. After demodulation, we have

$$
\begin{aligned}
I[k] &= \frac{2}{N}\sum_{n=Nk}^{N(k+1)-1} LO_I[n]\cdot S_1[n] \\
&= \frac{2}{N}\sum_{n=Nk}^{N(k+1)-1} \cos(2\pi fnT_s - k\Phi_{LO})\cdot\left[D[n]\cos(2\pi f_c nT_s + \phi[n])\right. \\
&\quad \left. + u_I'[n]\cos(2\pi f_c nT_s + \phi[n]) + u_Q'[n]\sin(2\pi f_c nT_s + \phi[n])\right] \\
&= \frac{1}{N}\sum_{n=Nk}^{N(k+1)-1} D[n]\cos\Phi[n] + u_I'[n]\cos\Phi[n] + u_Q'[n]\sin\Phi[n] \\
&\quad + high\ \ frequency\ \ terms,
\end{aligned}
$$

where

$$\Phi[n] = 2\pi\Delta fnT_s + k\Phi_{LO} + \phi[n] \tag{3.2-6}$$

and $\Delta f = f_c - f$. As we neglect high frequency part after integration and assume that $D[n]$ are constant over $[kT,(k+1)T) = [kNT_s,(k+1)NT_s)$, i. e., $D[n] = D'[k]$, where n = Nk, Nk+1, Nk+2…N(k+1)-1, and then

$$I[k] = D'[k]\cos\Phi'[k] + u_I[k]\cos\Phi'[k] + u_Q[k]\sin\Phi''[k] \tag{3.2-7}$$

where

$$\cos\Phi'[k] = \frac{1}{N}\sum_{n=Nk}^{N(k+1)-1}\cos\Phi[n], \tag{3.2-8}$$

$$\sin\Phi''[k] = \frac{1}{N}\sum_{n=Nk}^{N(k+1)-1}\sin\Phi[n]. \tag{3.2-9}$$

$$u_I[k]\cos\Phi'[k] = \frac{1}{N}\sum_{n=Nk}^{N(k+1)-1} u_I'[n]\cos\Phi[n],$$

$$u_Q[k]\sin\Phi''[k] = \frac{1}{N}\sum_{n=Nk}^{N(k+1)-1} u_Q'[n]\sin\Phi[n].$$

Similarly, we have the quadrature term

$$Q[k] = D'[k]\sin\Phi''[k] + u_I[k]\sin\Phi''[k] - u_Q[k]\cos\Phi'[k]. \tag{3.2-10}$$

The carrier phase discriminator is given by

$$\begin{aligned}\hat{\Phi}[k] &= \tan^{-1}\frac{Q[k]}{I[k]} \\ &= \tan^{-1}\frac{D[k]\sin\Phi'[k]+u_I[k]\sin\Phi'[k]-u_Q[k]\cos\Phi'[k]}{D[k]\cos\Phi'[k]+u_I[k]\cos\Phi'[k]+u_Q[k]\sin\Phi'[k]}\end{aligned} \tag{3.2-11}$$

Suppose $\Phi'[k] = \Phi''[k]$. As we neglect noise effect, from Eq. (3.2-6), Eq (3.2-8) and Eq (3.2-9), we have

$$\begin{aligned}\hat{\Phi}[k] &= \Phi'[k] \\ &= 2\pi\Delta fkT + k\Phi_{LO} + \bar{\phi}[k],\end{aligned} \tag{3.2-12}$$

From Eq. (3.2-12), the phase discriminator $\hat{\Phi}[k]$ consists of three components:

(i) $2\pi\Delta fkT$: frequency offset component,
(ii) $k\Phi_{LO}$: the beginning phase offset error of pre-established carrier table,
(iii) $\bar{\phi}[k]$: phase error component.

The frequency offset component changes very slowly compared with the phase error component. As we implement FLL in PCPC structure as shown in Figure 3.2-3(b), the output of H1 is given by

$$\begin{aligned}O_{H1}[k] &= \hat{\Phi}[k] - \hat{\Phi}[k-1] \\ &= 2\pi\Delta fT + \Phi_{LO} + \bar{\phi}[k] - \bar{\phi}[k-1].\end{aligned} \tag{3.2-13}$$

Since $\bar{\phi}[k] - \bar{\phi}[k-1]$ can be regarded as a high frequency term and would be removed after LPF H2, the output of H2 is given by

$$O_{H2}[k] = 2\pi\Delta fT + \Phi_{LO} \tag{3.2-14}$$

From Eq. (3.2-14), the estimated frequency adjustment is given by

$$\Delta\hat{f} = \frac{O_{H2}[k] - \Phi_{LO}}{2\pi T}. \tag{3.2-15}$$

We utilize Eq. (3.2-15) to adapt local carrier frequency as shown in Figure 3.2-3(b).

The frequency response of the proposed structure after phase discriminator is characterized by

$$H_4(z)\left[(\theta_i(z)-\theta_o(z))H_3(z)+\theta_i(z)H_1(z)H_2(z)\right]=\theta_o(z) \qquad (3.2\text{-}16)$$

From Eq. (3.2-16), the overall system response is given by

$$\frac{\theta_0(z)}{\theta_i(z)}=H(z)=\frac{H_4(z)\left[H_3(z)+H_1(z)H_2(z)\right]}{1+H_3(z)H_4(z)}$$

$$=\frac{z^{-1}\left[b+k_1+k_2-(2b+k_1+ak_1+ak_2)z^{-1}+(ak_1+b)z^{-2}\right]}{(1-az^{-1})\left[1+(k_1+k_2-2)z^{-1}+(1-k_1)z^{-2}\right]} \qquad (3.2\text{-}17)$$

We choose a satisfying $|a|<1$, and select k_1 and k_2 carefully so that all the poles of H(z) fall in the unit circle. This condition guarantees the stability of the system.

3.2.4 Implementation issues

1) FLL scheme:

As mentioned above, the output of H2 can be used to estimate frequency variation directly. The sources of frequency variation include motion of satellite or user, clock drift and local carrier frequency bias etc. It is worth to mention that the phase offset effect of local carrier table must be considered in order to attain correct frequency variation. The effect is induced because the beginning phase of a pre-established carrier table is always zero while the local carrier of the following interval may have a nonzero beginning phase, i.e., the integration interval may be not the multiple of carrier wavelength. A schematic plot of this effect is shown in Figure 3.2-5.

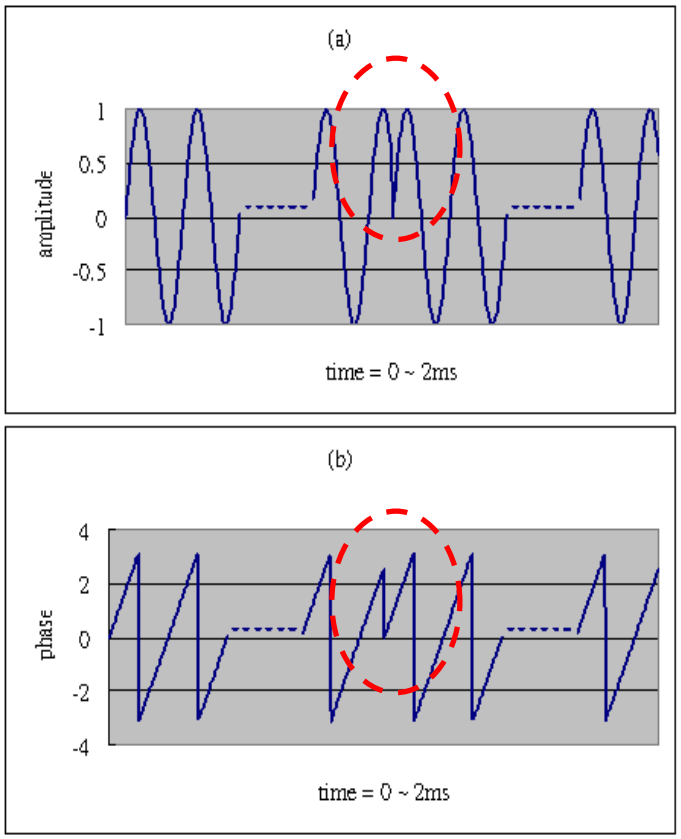

Figure 3.2-5 An example of the beginning phase offset problem for a pre-established carrier table with integration interval 1 ms

2) Range of phase for each stage:

Since the phase compensation is implemented after ATAN phase detector, the phase range of each stage must be taken care carefully in order to avoid navigation bit transition effect and 2π transition influence on phase estimate.

4. Carrier Phase Discriminator

As the feasible PCPC structure for 1-bit SGR is provided in the previous section, we are ready to propose a computationally efficient phase discriminator as follows.

4.1 Conventional phase discriminators

The arctangent phase discriminator (APD) is one of the most widely used in PLL tracking loops since it's an optimal detector in analog signal cases with additive-white-Gaussian-noise (AWGN).[9].

The arctangent phase discriminator (APD) is a high precision phase detector in analog signal cases. However, the heavy computation load with the arctangent discriminator is sometimes a concerned issue in some digital implementation receivers. A number of phase discriminators are proposed to approximate arctangent in order to save computation[2] [3]. Figure 4.1-1 compares the proposed NB-DPD with conventional phase discriminators.

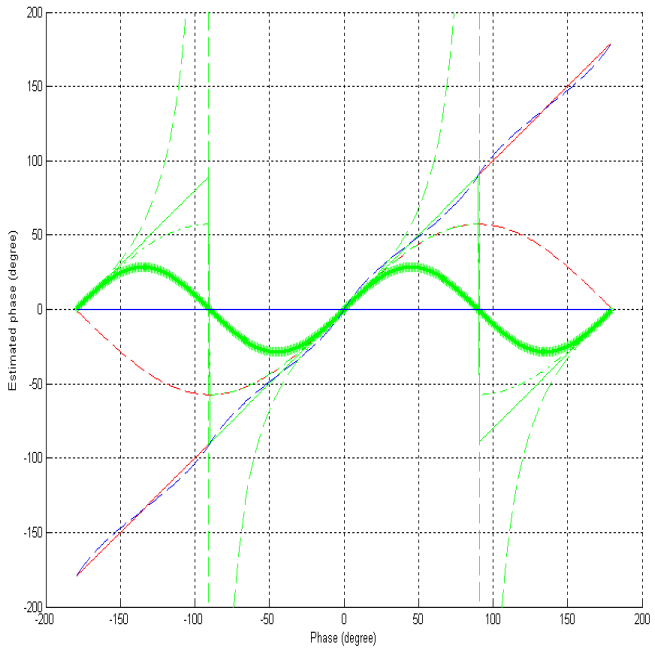

Figure 4.1-1 Comparison of ATAN2 (red solid) with ATAN (green solid), Qp (red dashed), Qp/Ip (green dashed), sign(Ip)Qp (green dash-dotted), IpQp, (green starred) and NB-DPD (blue dashed) without noise.

Another issue with arctangent is the quantization loss. When applying arctangent in digital cases with few bits ADC, the accuracy will degrade greatly due to high quantization loss. A novel phase discriminator, called digital phase discriminator (DPD), is proposed to mitigate quantization loss by Chang and Kao[1]. The DPD discriminator has been shown to achieve much higher accuracy than the arctangent discriminator in 1-bit software-defined receiver up to several orders in high SNR cases. However, the DPD does not perform well in low SNR environments such as global navigation satellite system (GNSS) applications because of its sensitivity to the noise. A modified DPD, called noise-balanced digital phase discriminator (NB-DPD), which works in both noiseless and noisy environments is proposed in the following sections.

4.2 Proposed noise-balanced digital phase discriminator (NB-DPD)

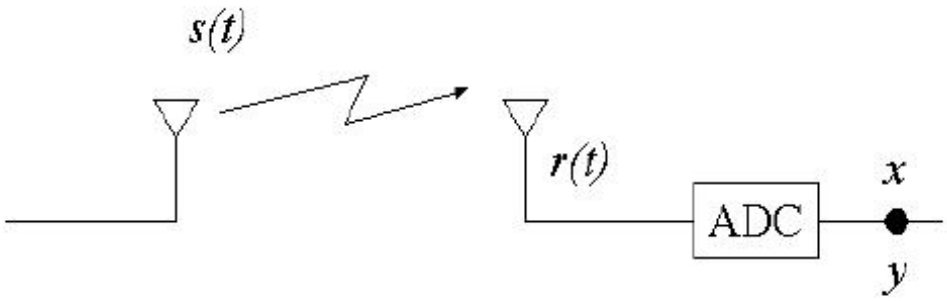

Figure. 4.2-1. Schematic plot of the system

A schematic plot of the system is shown in Figure 4.2-1. First, consider the transmitted signal given by

$$s(t) = A\sin(2\pi f_c t + \theta) \tag{4.2-1}$$

where f_c is the carrier frequency, and the received signal is given by

$$r(t) = A\sin(2\pi f_c t + \theta) + u(t) \tag{4.2-2}$$

where u(t) is the environmental noise. In noiseless environments, the output signal of 1-bit ADC is given by

$$x[n] = \mathrm{sgn}[\sin(2\pi f_c n T_s + \theta)] = \mathrm{sgn}[s(nT_s)] = \mathrm{sgn}[s[n]] \tag{4.2-3}$$

where T_s is the sampling period and sgn(·) denotes the polarity function, i. e., sgn[x] = 1 if x $\geq$ 0 and sgn[x] = −1 if x $\leq$ 0. We can treat sgn[$s(t)$] as a square wave and x[n] as samples on this square wave. Similarly, in noisy environments, the output signal of 1-bit ADC is given by

$$y[n] = \mathrm{sgn}[s[n] + u[n]] \tag{4.2-4}$$

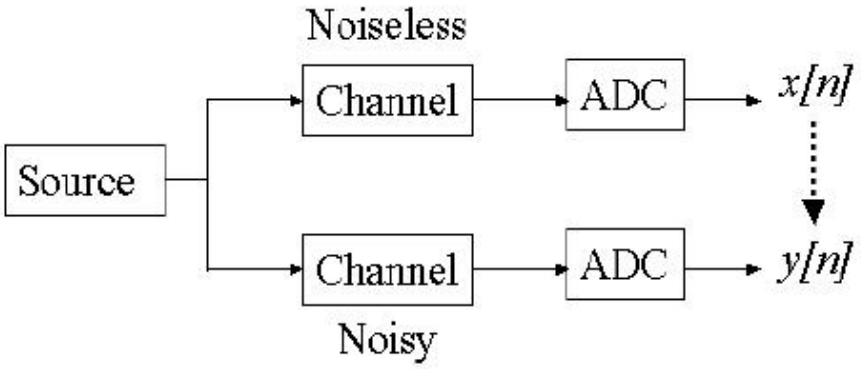

Figure 4.2- 2. The block diagram expressing noiseless channel and noisy channel

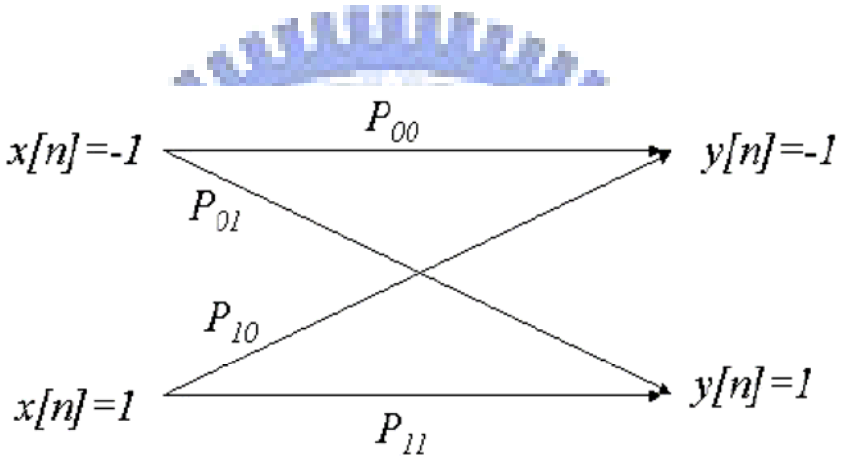

Figure 4.2-3. Binary probability model

The overall system can be explained in Figure 4.2-2. In order to analyze the DPD in noisy environments, we need to establish the connection between x[n] and y[n]. This can be achieved through probability approach. First, we have the following conditional probabilities:

$$P_{00} = P(y[n] = -1 \mid \ x[n] = -1), \tag{4.2-5}$$

$$P_{01} = P(y[n] = 1 \mid \ x[n] = -1), \tag{4.2-6}$$

$$P_{10} = P(y[n] = -1 \mid \ x[n] = 1), \tag{4.2-7}$$

$$P_{11} = P(y[n] = 1 \mid \ x[n] = 1), \tag{4.2-8}$$

Using Eqs.(4.2-5)-(4.2-8), the binary probability model is established as shown in Figure 4.2-3. Next, we consider u(t) as a zero-mean additive white Gaussian noise (AWGN), it is reasonable to assume that

$$P_{00} = P_{11}, \quad P_{01} = P_{10} < \frac{1}{2} \tag{4.2-9}$$

With Eq. (4.2-9), the probability model in Figure 4.2-3 becomes a binary symmetrical structure. Hence the proposed modified DPD is called noise-balanced digital phase discriminator (NB-DPD), which assumes the noise effect is "balanced" regarding in-phase channel and quadrature channel at every sample of the incoming signal.

Furthermore, similar to the digital perspective in Eq. (4.2-3), we also regard local reference signals as samples on square wave given by

$$LO_I[n] = \mathrm{sgn}[\sin(2\pi f_\omega n T_s)], \tag{4.2-10}$$

$$LO_Q[n] = \mathrm{sgn}[\cos(2\pi f_\omega n T_s)], \tag{4.2-11}$$

where f_ω is the local carrier frequency. From the Eq. (4.2-3) ~ Eq. (4.2-11), the NB-DPD model is provided in Figure 4.2-4.

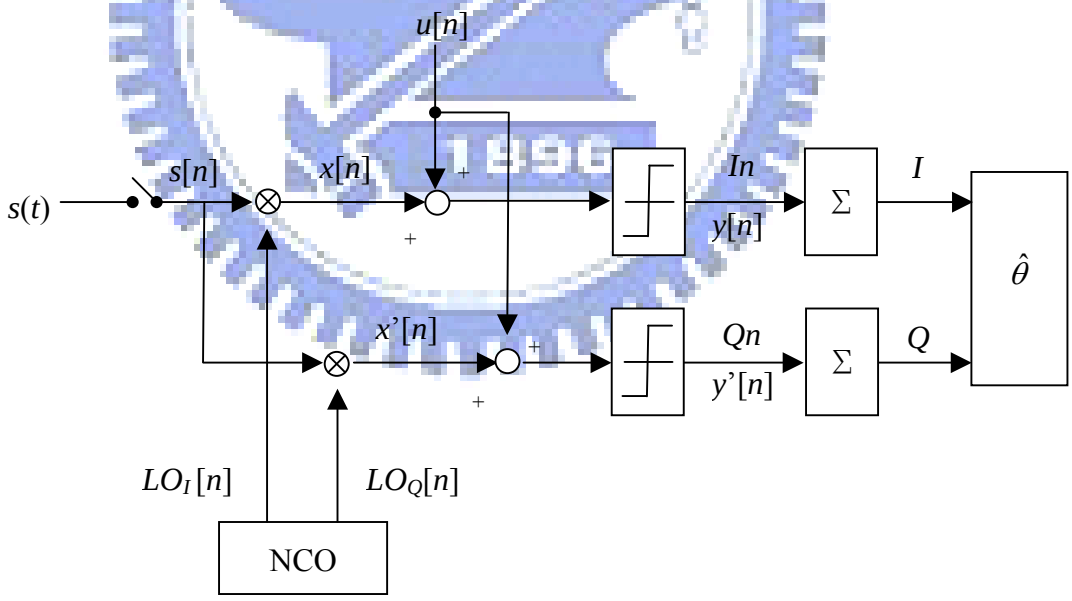

Figure 4.2-4: The NB-DPD signal model

The DPD approach is based on digital perspective, which derives received carrier phase by comparing the time delay between received signal and local reference signal as shown in Figure 4.2-5.

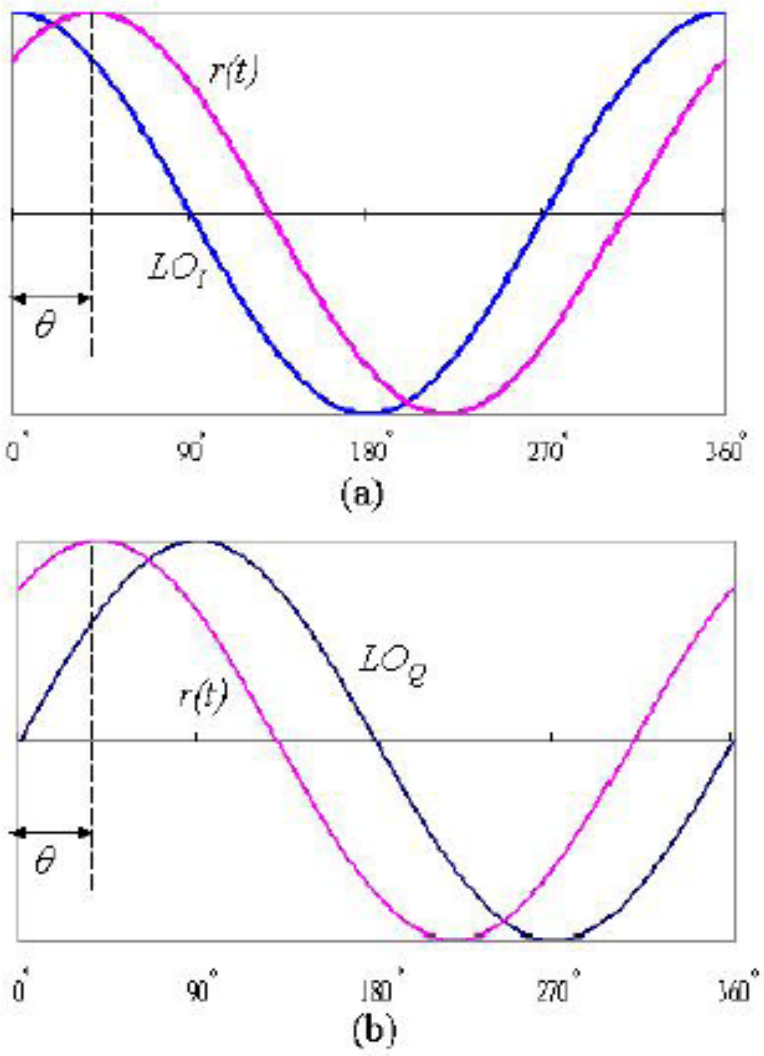

Figure 4.2-5: The schematic plot of time delay and corresponding phase difference θ between the received signal and local reference signals in (a) in-phase channel and (b) quadrature channel, respectively.

Let T be the observation time and N = T/Ts be the number of samples within T. Assume $f_c = f_\omega$ and $\phi_n = 2\pi f_c n T_s$, where n = 0, 1, 2..., N−1. we have

$$I_n = y[n] = \mathrm{sgn}[x[n] + u[n]], \tag{4.2-12}$$

$$Q_n = y'[n] = \mathrm{sgn}[x'[n] + u[n]], \tag{4.2-13}$$

$$I = \sum_{n=0}^{N-1} I_n = \sum_{n=0}^{N-1} y[n] \tag{4.2-14}$$

$$Q = \sum_{n=0}^{N-1} Q_n = \sum_{n=0}^{N-1} y'[n] \tag{4.2-15}$$

Let N_+ denote the number of samples with $I_n = 1$, N_- denote the number of samples with $I_n = -1$, N'_+ denote the number of samples with $Q_n = 1$ and N'_- denote the number of samples with $Q_n = -1$. Then we have

$$I = N_+ - N_-, \quad Q = N'_+ - N'_- \tag{4.2-16}$$

Suppose the observed samples satisfy the uniformity condition, i. e., ϕ_0, ϕ_1, $\cdots$, ϕ_{N-1} are uniformly distributed over [0, 2π].[1] Firstly let's consider the case that the phase difference θ is in the range of [0, π /2], i.e., $0 \leqq \theta < \pi/2$. With respect to the time delay between the received signal and local reference signal as shown in Figure 4.2-5 and the binary probability model as in Figure 4.2-3, we have N_- and N_+ for I-channel as follows

$$\begin{aligned} N_- &= \frac{\theta}{\pi} N(1-P_{01}) + (\frac{\pi-\theta}{\pi}) NP_{10} \\ &= N\left[\frac{\theta}{\pi} + \frac{\pi-2\theta}{\pi} P_e\right], \end{aligned} \tag{4.2-17}$$

$$\begin{aligned} N_+ &= \frac{\pi-\theta}{\pi} N(1-P_{10}) + \frac{\theta}{\pi} NP_{01} \\ &= N\left[\frac{\pi-\theta}{\pi} + \frac{2\theta-\pi}{\pi} P_e\right], \end{aligned} \tag{4.2-18}$$

where, $P_e = P_{10} = P_{01}$. Similarly, for Q-channel, we have

$$\begin{aligned} N'_- &= (\frac{1}{2} - \frac{\theta}{\pi}) N(1-P_{01}) + (\frac{1}{2} + \frac{\theta}{\pi}) NP_{10}, \\ &= N\left[(\frac{1}{2} - \frac{\theta}{\pi}) + \frac{2\theta}{\pi} P_e\right], \end{aligned} \tag{4.2-19}$$

$$\begin{aligned} N'_+ &= (\frac{1}{2} - \frac{\theta}{\pi}) NP_{01} + (\frac{1}{2} + \frac{\theta}{\pi}) N(1-P_{10}), \\ &= N\left[(\frac{1}{2} + \frac{\theta}{\pi}) - \frac{2\theta}{\pi} P_e\right]. \end{aligned} \tag{4.2-20}$$

From Eqs.(4.2-16)-(4.2-20), we have

$$I = N_+ - N_- = \frac{N}{\pi}(\pi - 2\theta)(1 - 2P_e), \tag{4.2-21}$$

$$Q = N'_+ - N'_- = \frac{2N\theta}{\pi}(1 - 2P_e), \tag{4.2-22}$$

Combining Eq. (4.2-21) and Eq. (4.2-22), we obtain

$$\frac{I}{|I| + |Q|} = 1 - \frac{2\theta}{\pi} \tag{4.2-23}$$

As for other phase ranges of θ, we have

when $\pi/2 \le \theta < \pi$,

$$\frac{I}{|I| + |Q|} = 1 - \frac{2\theta}{\pi} \tag{4.2-24}$$

when $-\pi \le \theta < 0$,

$$\frac{I}{|I| + |Q|} = 1 + \frac{2\theta}{\pi} \tag{4.2-25}$$

From Eq. (4.2-23), (4.2-24) and (4.2-25), we have

$$|\theta| = \frac{\pi}{2}\left(1 - \frac{I}{|I| + |Q|}\right) \tag{4.2-26}$$

As for the polarity ambiguity of θ, it can be resolved by

$$\mathrm{sgn}[\theta] = \mathrm{sgn}[Q] \tag{4.2-27}$$

which is obtained from Eq. (4.2-22). Hence we have

$$\hat{\theta} = \mathrm{sgn}[Q]\frac{\pi}{2}\left(1 - \frac{I}{|I| + |Q|}\right) \tag{4.2-28}$$

Note that the phase estimate in Eq. (4.2-28) does not depend on noise.

The above approach is developed in a more intuitive way and can be verified by the probabilistic approach in [11].

4.3 Analysis of NB-DPD estimator

Recall the signals and parameters as follows.

1) Received signal and local carriers:

$$r(t) = A\sin(2\pi f_c t + \theta) + u(t)$$
$$LO_I(t) = \sin(2\pi f_\omega t)$$
$$LO_Q(t) = \cos(2\pi f_\omega t)$$

2) After 1-bit ADC:

Assume $f_c = f_\omega$ and $\phi_n = 2\pi f_c n T_s$, $n \in [0, N-1]$, N is the number of total samples in observation period, then we have:

$$\text{sgn}[r(nT_s)] = \text{sgn}[A\sin(\phi_n + \theta) + u(nT_s)]$$
$$\text{sgn}[LO_I(nT_s)] = \text{sgn}[\sin(\phi_n)]$$
$$\text{sgn}[LO_Q(nT_s)] = \text{sgn}[\cos(\phi_n)]$$

3) Correlator output:

$$I_n = \text{sgn}[r(nT_s)] \cdot \text{sgn}[LO_I(nT_s)]$$
$$= \text{sgn}[A\sin(\phi_n + \theta) + u(nT_s)] \cdot \text{sgn}[\sin(\phi_n)]$$
$$Q_n = \text{sgn}[r(nT_s)] \cdot \text{sgn}[LO_Q(nT_s)]$$
$$= \text{sgn}[A\sin(\phi_n + \theta) + u'(nT_s)] \cdot \text{sgn}[\cos(\phi_n)]$$

4) SNR and σ:

σ denotes the standard deviation of $u(nT_s)$

$$SNR = \frac{A^2}{2\sigma^2}$$

$$\Rightarrow \sigma = \frac{A}{\sqrt{2SNR}}$$

4.3.1 Statistical properties of I_n and Q_n [11]

The prabability-density-function (pdf), mean, and variance of the random variables I_n and Q_n are derived below.

4.3.1.1 I_n

1). when $\phi_n \in [0, \pi)$, we have $\sin(\phi_n) \geq 0$

(a) Conditional pdf:

$$P(I_n = 1|\theta) = P(\sin(\phi_n + \theta) + u(nT_s) \geq 0|\theta)$$
$$= 1 - Q(\frac{A \cdot \sin(\phi_n + \theta)}{\sigma}) = 1 - Q(\sqrt{2SNR} \cdot \sin(\phi_n + \theta)) \quad (4.3.1\text{-}1)$$

$$P(I_n = -1|\theta) = Q(\sqrt{2SNR} \cdot \sin(\phi_n + \theta)) \quad (4.3.1\text{-}2)$$

(b) Mean:

$$\mu_{I_n} = 1 \times P(I_n = 1|\theta) - P(I_n = -1|\theta) = 1 - 2Q(\sqrt{2SNR} \cdot \sin(\phi_n + \theta)) \quad (4.3.1\text{-}3)$$

(c) Variance:

$$\sigma_{I_n}^2 = E[I_n^2] - \mu_{I_n}^2 = 4Q(\sqrt{2SNR} \cdot \sin(\phi_n + \theta)) - 4[Q(\sqrt{2SNR} \cdot \sin(\phi_n + \theta))]^2$$
$$= 4Q(\sqrt{2SNR} \cdot \sin(\phi_n + \theta)) \cdot [1 - Q(\sqrt{2SNR} \cdot \sin(\phi_n + \theta))] \quad (4.3.1\text{-}4)$$

2). when $\phi_n \in [-\pi, 0)$, we have $\sin(\phi_n) \leq 0$

(a) Conditional pdf:

$$P(I_n = 1|\theta) = P(\sin(\phi_n + \theta) + u(nT_s) \leq 0|\theta)$$
$$= Q(\sqrt{2SNR} \cdot \sin(\phi_n + \theta)) \quad (4.3.1\text{-}5)$$

$$P(I_n = -1|\theta) = 1 - Q(\sqrt{2SNR} \cdot \sin(\phi_n + \theta)) \quad (4.3.1\text{-}6)$$

(b) Mean:

$$\mu_{I_n} = 1 \times P(I_n = 1|\theta) - P(I_n = -1|\theta) = -1 + 2Q(\sqrt{2SNR} \cdot \sin(\phi_n + \theta)) \quad (4.3.1\text{-}7)$$

(c) Variance:

$$\sigma_{I_n}^2 = E[I_n^2] - \mu_{I_n}^2 = 4Q(\sqrt{2SNR}\cdot\sin(\phi_n+\theta)) - 4[Q(\sqrt{2SNR}\cdot\sin(\phi_n+\theta))]^2$$

$$= 4Q(\sqrt{2SNR}\cdot\sin(\phi_n+\theta))\cdot[1-Q(\sqrt{2SNR}\cdot\sin(\phi_n+\theta))] \qquad (4.3.1\text{-}8)$$

where Q-function is given by

$$Q(z) = \frac{1}{\sqrt{2\pi}}\int_z^\infty e^{-\frac{x^2}{2}}dx$$

4.3.1.2 Q_n

1). when $\phi_n \in [\frac{-\pi}{2}, \frac{\pi}{2})$, we have $\cos(\phi_n) \geq 0$

(a) Conditional pdf:

$$P(Q_n = 1|\theta) = P(\sin(\phi_n+\theta) + u'(nT_s) \geq 0|\theta)$$

$$= 1 - Q(\frac{A\cdot\sin(\phi_n+\theta)}{\sigma}) = 1 - Q(\sqrt{2SNR}\cdot\sin(\phi_n+\theta)) \qquad (4.3.1\text{-}9)$$

$$P(Q_n = -1|\theta) = Q(\sqrt{2SNR}\cdot\sin(\phi_n+\theta)) \qquad (4.3.1\text{-}10)$$

(b) Mean:

$$\mu_{Q_n} = 1\times P(Q_n = 1|\theta) - P(Q_n = -1|\theta) = 1 - 2Q(\sqrt{2SNR}\cdot\sin(\phi_n+\theta)) \qquad (4.3.1\text{-}11)$$

(c) Variance:

$$\sigma_{Q_n}^2 = E[Q_n^2] - \mu_{Q_n}^2 = 4Q(\sqrt{2SNR}\cdot\sin(\phi_n+\theta)) - 4[Q(\sqrt{2SNR}\cdot\sin(\phi_n+\theta))]^2$$

$$= 4Q(\sqrt{2SNR}\cdot\sin(\phi_n+\theta))\cdot[1-Q(\sqrt{2SNR}\cdot\sin(\phi_n+\theta))] \qquad (4.3.1\text{-}12)$$

2). when $\phi_n \in [\frac{\pi}{2}, \pi)$ or $\phi_n \in [-\pi, \frac{-\pi}{2})$, we have $\cos(\phi_n) \leq 0$

(a) Conditional pdf:

$$P(Q_n = 1|\theta) = P(\sin(\phi_n+\theta) + u(nT_s) \leq 0|\theta)$$

$$= Q(\sqrt{2SNR} \cdot \sin(\phi_n + \theta)) \tag{4.3.1-13}$$

$$P(Q_n = -1|\theta) = 1 - Q(\sqrt{2SNR} \cdot \sin(\phi_n + \theta)) \tag{4.3.1-14}$$

(b) Mean:

$$\mu_{Q_n} = 1 \times P(Q_n = 1|\theta) - P(Q_n = -1|\theta) = -1 + 2Q(\sqrt{2SNR} \cdot \sin(\phi_n + \theta)) \tag{4.3.1-15}$$

(c) Variance:

$$\sigma_{Q_n}^2 = E[Q_n^2] - \mu_{Q_n}^2 = 4Q(\sqrt{2SNR} \cdot \sin(\phi_n + \theta)) - 4[Q(\sqrt{2SNR} \cdot \sin(\phi_n + \theta))]^2$$

$$= 4Q(\sqrt{2SNR} \cdot \sin(\phi_n + \theta)) \cdot [1 - Q(\sqrt{2SNR} \cdot \sin(\phi_n + \theta))] \tag{4.3.1-16}$$

From Eq.(4.3.1-8) and Eq.(4.3.1-16), note that the variance of I_n is same as Q_n.

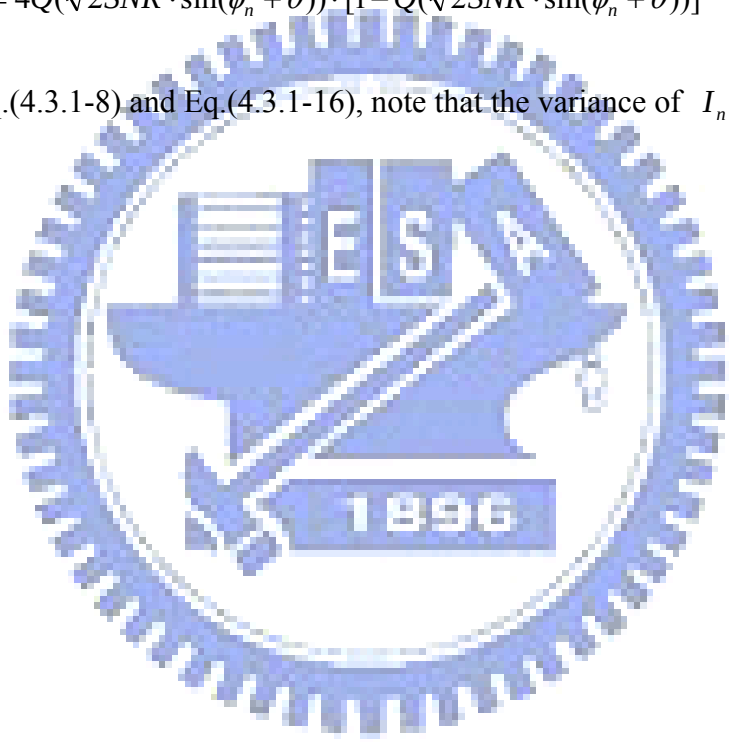

4.3.2 Statistical properties of I_{p_i} and Q_{p_i} groups

1). I_{p_i} and Q_{p_i} :

Suppose $\frac{f_c}{f_s} = K + \frac{L}{P}$, where f_s is sampling rate, $P > L$, P and L are relative prime integers. It can be shown that $(\phi_0, \phi_1, ...\phi_{p-1})$ are uniformly distributed over $[0, 2\pi]$.[1]

Define $I_{p_i} = \{I_n \mid n \ \ MOD \ \ P \ = p_i\}$, $Q_{p_i} = \{Q_n \mid n \ \ MOD \ \ P \ = p_i\}$, where, $0 \le n \le N-1$, $i = 0,1,2.....P-1$, and $p_i = i$. Then the components of I_{p_i} group are i.i.d., and so are the components of Q_{p_i} group, and we have

$$\sigma^2_{I_{p_i}} = \sigma^2_{Q_{p_i}} \quad . \text{(4.3.2-1)}$$

2). I_{Gp_i} and Q_{Gp_i}

Suppose we have $N = P \cdot M$ samples,

$$\text{Define } I_{Gp_i} = \frac{1}{M} \cdot \sum_{m=0}^{M-1} I_{n=mP+p_i} , \quad \text{(4.3.2-2)}$$

$$Q_{Gp_i} = \frac{1}{M} \cdot \sum_{m=0}^{M-1} Q_{n=mP+p_i} , \quad \text{(4.3.2-3)}$$

(a) pdf:

$$\text{Let} \quad b(k, M, p_{I_{p_i}}) \equiv \binom{M}{k} p^k_{I_{p_i}} (1 - p_{I_{p_i}})^{M-k} \quad \text{(4.3.2-4)}$$

$$b(k, M, p_{Q_{p_i}}) \equiv \binom{M}{k} p^k_{Q_{p_i}} (1 - p_{Q_{p_i}})^{M-k} \quad \text{(4.3.2-5)}$$

where $p_{I_{p_i}} = P(I_{p_i} = 1 | \theta)$, $p_{Q_{p_i}} = P(Q_{p_i} = 1 | \theta)$

$$\Rightarrow P(I_{Gp_i} = x_k) = b(k, M, p_{I_{p_i}}) \quad \text{(4.3.2-6)}$$

$$P(Q_{Gp_i} = x_k) = b(k, M, p_{Q_{p_i}}) , \quad \text{(4.3.2-7)}$$

where $x_k = -1 + \frac{2k}{M}, \quad k = 0,1,2,....M$

(b) Mean:

$$\mu_{I_{Gp_i}} = E[I_{Gp_i}] = E[\frac{1}{M} \cdot \sum_{m=0}^{M-1} I_{n=mP+p_i}] = E[I_{p_i}] = \mu_{I_{p_i}} \tag{4.3.2-8}$$

$$\mu_{Q_{Gp_i}} = E[Q_{Gp_i}] = E[\frac{1}{M} \cdot \sum_{m=0}^{M-1} Q_{n=mP+p_i}] = E[Q_{p_i}] = \mu_{Q_{p_i}} \tag{4.3.2-9}$$

(c) Variance:

I_{p_i}'s are independent, $\Rightarrow \sigma^2_{I_{Gp_i}} = \frac{1}{M^2} \cdot \sum_{m=0}^{M-1} \sigma^2_{I_{n=mP+p_i}} = \frac{\sigma^2_{I_{p_i}}}{M}$ (4.3.2-10)

Q_{p_i}'s are independent, $\Rightarrow \sigma^2_{Q_{Gp_i}} = \frac{1}{M^2} \cdot \sum_{m=0}^{M-1} \sigma^2_{Q_{n=mP+p_i}} = \frac{\sigma^2_{Q_{p_i}}}{M}$ (4.3.2-11)

Since $\sigma^2_{I_{p_i}} = \sigma^2_{Q_{p_i}}, \Rightarrow \sigma^2_{I_{Gp_i}} = \sigma^2_{Q_{Gp_i}}$ (4.3.2-12)

(d) According to Central Limit Theorem (CLT), I_{Gp_i} and Q_{Gp_i} approximate to Gaussian distribution when N is sufficiently large.i.e.,

$I_{Gp_i} \sim \mathrm{N}(\mu_{I_{p_i}}, \sigma^2_{I_{Gp_i}})$ and $Q_{Gp_i} \sim \mathrm{N}(\mu_{Q_{p_i}}, \sigma^2_{Q_{Gp_i}})$ when $N \to \infty$.

4.3.3 Statistical properties of I and Q

Define $I = \frac{1}{P} \cdot \sum_{p_i=0}^{P-1} I_{Gp_i}$, $Q = \frac{1}{P} \cdot \sum_{p_i=0}^{P-1} Q_{Gp_i}$ (4.3.3-1)

The range of I and Q is $x \in [-1,1]$, $x = -1 + \frac{2k}{N}$, where $k \in [0, N]$, k is integer.

(a) pdf of I and Q

Assume I_{Gp_i} and I_{Gp_j} are independent, where $i \neq j$, we have

$$\Phi_I(\omega) = \frac{1}{P} \Phi_{I_{Gp_0}}(\omega) \cdot \Phi_{I_{Gp_1}}(\omega) \ldots \Phi_{I_{Gp_{p-1}}}(\omega) \quad (4.3.3\text{-}2)$$

$$\Rightarrow f_I(i) = \frac{1}{P} f_{I_{Gp_0}}(i_{Gp_0}) * f_{I_{Gp_1}}(i_{Gp_1}) * \ldots\ldots * f_{I_{Gp_{p-1}}}(i_{Gp_{p-1}}) \quad (4.3.3\text{-}3)$$

Similarly, assume Q_{Gp_i} and Q_{Gp_j} are independent, we have

$$\Phi_Q(\omega) = \frac{1}{P} \Phi_{Q_{Gp_0}}(\omega) \cdot \Phi_{Q_{Gp_1}}(\omega) \ldots \Phi_{Q_{Gp_{p-1}}}(\omega) \quad (4.3.3\text{-}4)$$

$$\Rightarrow f_Q(q) = \frac{1}{P} f_{Q_{Gp_0}}(q_{Gp_0}) * f_{Q_{Gp_1}}(q_{Gp_1}) * \ldots\ldots * f_{Q_{Gp_{p-1}}}(q_{Gp_{p-1}}) \quad (4.3.3\text{-}5)$$

(b) Assume I_{Gp_i} and I_{Gp_j} are independent, as well as Q_{Gp_i} and Q_{Gp_j}, where $i \neq j$.

Since I_{Gp_i} and Q_{Gp_i} approximate to Gaussian distribution when N is sufficiently large, we have

$$I \sim \mathrm{N}(\mu_I, \sigma_I^2), \text{ i.e., } I \sim \mathrm{N}\left(\frac{1}{P}\sum_{p_i=0}^{p-1}\mu_{I_{Gp_i}}, \frac{1}{P^2}\sum_{p_i=0}^{p-1}\sigma_{I_{Gp_i}}^2\right) \quad (4.3.3\text{-}6)$$

$$Q \sim \mathrm{N}(\mu_Q, \sigma_Q^2), \text{ i.e., } Q \sim \mathrm{N}\left(\frac{1}{P}\sum_{p_i=0}^{p-1}\mu_{Q_{Gp_i}}, \frac{1}{P^2}\sum_{p_i=0}^{p-1}\sigma_{Q_{Gp_i}}^2\right) \quad (4.3.3\text{-}7)$$

From Eq.(4.3.3-6) and Eq.(4.3.37), note that σ_I^2 and σ_Q^2 are independent of θ.

And from Eq.(4.3.2-12), since $\sigma_{I_{GPi}}^2 = \sigma_{Q_{Gp_i}}^2$, we have

$$\sigma_I^2 = \sigma_Q^2 \quad (4.3.3\text{-}8)$$

4.3.4 Statistical properties of $|I|$ and $|Q|$

Let $Y = |I|$, $V = |Q|$, then Y and V are Rician distribution random variables.

(a) pdf:

$$f_Y(y) = \begin{cases} f_I(y) + f_I(-y) & ; y \geq 0 \\ 0 & ; y < 0 \end{cases} \tag{4.3.4-1}$$

$$f_V(v) = \begin{cases} f_Q(v) + f_Q(-v) & ; v \geq 0 \\ 0 & ; v < 0 \end{cases} \tag{4.3.4-2}$$

Since $N \to \infty$, $I \sim \mathrm{N}(\mu_I, \sigma_I^2)$, $Q \sim \mathrm{N}(\mu_Q, \sigma_Q^2)$, where, $\sigma_I^2 = \sigma_Q^2$, i.e.,

$$f_I(i) = \frac{1}{\sqrt{2\pi\sigma_I^2}} \cdot \exp\left(\frac{-(i-\mu_I)^2}{2\sigma_I^2}\right) \tag{4.3.4-3}$$

$$f_Q(q) = \frac{1}{\sqrt{2\pi\sigma_Q^2}} \cdot \exp\left(\frac{-(q-\mu_Q)^2}{2\sigma_Q^2}\right) \tag{4.3.4-4}$$

$$\Rightarrow f_Y(y) = \begin{cases} \frac{\sqrt{2}}{\sqrt{\pi\sigma_I^2}} \cdot \exp\left(-\frac{y^2+\mu_I^2}{2\sigma_I^2}\right) \cdot \cosh\left(\frac{y\mu_I}{\sigma_I^2}\right) & ; y \geq 0 \\ 0 & ; y < 0 \end{cases} \tag{4.3.4-5}$$

$$f_V(v) = \begin{cases} \frac{\sqrt{2}}{\sqrt{\pi\sigma_Q^2}} \cdot \exp\left(-\frac{v^2+\mu_Q^2}{2\sigma_Q^2}\right) \cdot \cosh\left(\frac{v\mu_Q}{\sigma_Q^2}\right) & ; v \geq 0 \\ 0 & ; v < 0 \end{cases} \tag{4.3.4-6}$$

(b) Mean:

The moment of a Rician random variable is given by [13]

$$E[R^k] = (2\sigma^2)^{\frac{k}{2}} \cdot \exp(\frac{-\mu^2}{2\sigma^2}) \cdot \frac{\Gamma(\frac{k+1}{2})}{\sqrt{\pi}} \cdot {}_1F_1(\frac{k+1}{2}; \frac{1}{2}; \frac{\mu^2}{2\sigma^2}) \qquad (4.3.4\text{-}7)$$

where, $\Gamma(z)$ is the gamma function, and ${}_1F_1(\alpha;\beta;\gamma)$ is the confluent hypergeometric function.

Since $\Gamma(1) = 1$, $\Gamma(1/2) = \sqrt{\pi}$, $\Gamma(3/2) = \sqrt{\pi}/2$,

$$\Rightarrow \mu_{|I|} = E[Y] = \frac{1}{\sqrt{\pi}} \cdot (2\sigma_I^2)^{\frac{1}{2}} \cdot \exp(\frac{-\mu_I^2}{2\sigma_I^2}) \cdot {}_1F_1(1; \frac{1}{2}; \frac{\mu_I^2}{2\sigma_I^2}) \qquad (4.3.4\text{-}8)$$

$$\mu_{|Q|} = E[V] = \frac{1}{\sqrt{\pi}} \cdot (2\sigma_Q^2)^{\frac{1}{2}} \cdot \exp(\frac{-\mu_Q^2}{2\sigma_Q^2}) \cdot {}_1F_1(1; \frac{1}{2}; \frac{\mu_Q^2}{2\sigma_Q^2}) \qquad (4.3.4\text{-}9)$$

(b) Variance:

$$\sigma_{|I|}^2 = E[Y^2] - \mu_{|I|}^2$$

$$= \sigma_I^2 \cdot \exp(\frac{-\mu_I^2}{2\sigma_I^2}) \cdot {}_1F_1(\frac{3}{2}; \frac{1}{2}; \frac{\mu_I^2}{2\sigma_I^2}) - \frac{2\sigma_I^2}{\pi} \cdot \exp(\frac{-\mu_I^2}{\sigma_I^2}) \cdot [{}_1F_1(1; \frac{1}{2}; \frac{\mu_I^2}{2\sigma_I^2})]^2 \qquad (4.3.4\text{-}10)$$

$$\sigma_{|Q|}^2 = E[V^2] - \mu_{|Q|}^2$$

$$= \sigma_Q^2 \cdot \exp(\frac{-\mu_Q^2}{2\sigma_Q^2}) \cdot {}_1F_1(\frac{3}{2}; \frac{1}{2}; \frac{\mu_Q^2}{2\sigma_Q^2}) - \frac{2\sigma_Q^2}{\pi} \cdot \exp(\frac{-\mu_Q^2}{\sigma_Q^2}) \cdot [{}_1F_1(1; \frac{1}{2}; \frac{\mu_Q^2}{2\sigma_Q^2})]^2 \qquad (4.3.4\text{-}11)$$

4.3.5 Statistical properties of $\frac{I}{|I|+|Q|}$

Let $X = \frac{I}{|I|+|Q|}$, the range of X is $x_k \in [-1,1]$, where $x_k = -1 + \frac{2k}{N}$, and $k = 0,1,2,....,N$. We have the cumulative-distribution-function (CDF) as follows:

$$F_X(x_k) = P[X \le x_k] = P[I \le x_k(|I|+|Q|)] = P[I - x_k|I| \le x|Q|] \qquad (4.3.5\text{-}1)$$

From Eq.(4.3.5-1), we may derive the pdf of X as follow:

1) Derivation conditioned on $|Q|$

(a) when $-1 \le x_k \le 0$, it implies $I \le 0$

$$F_X(x_k) = P[X \le x_k] = P[I(1+x_k) \le x_k \cdot |Q|] = P[I \le \frac{x_k}{1+x_k}|Q|]$$

$$= \sum_{q_j} F_I(\frac{x_k \cdot q_j}{1+x_k}) \cdot P[|Q| = q_j] \qquad (4.3.5\text{-}2)$$

when $N \to \infty$,

$$F_X(x) = \int_0^\infty F_I(\frac{xq}{1+x}) \cdot f_V(q)dq = \int_0^\infty [1 - Q(\frac{\frac{xq}{1+x} - \mu_I}{\sigma_I})] \cdot f_V(q)dq$$

$$= 1 - \int_0^\infty Q(\frac{\frac{xq}{1+x} - \mu_I}{\sigma_I}) \cdot f_V(q)dq \qquad (4.3.5\text{-}3)$$

where, $f_V(q) = \frac{\sqrt{2}}{\sqrt{\pi\sigma_Q^2}} \exp(-\frac{q^2+\mu_Q^2}{2\sigma_Q^2}) \cdot \cosh(\frac{q\mu_Q}{\sigma_Q^2})$,

$$Q(x) = \frac{1}{\sqrt{2\pi}} \int_x^\infty \exp(-\frac{y^2}{2})dy, \text{ and } V = |Q|$$

$$f_X(x) = \frac{d}{dx} F_X(x) = \int_0^{\infty} \frac{\partial}{\partial x}[1 - Q(\frac{\frac{xq}{1+x} - \mu_I}{\sigma_I})] \cdot f_V(q) dq \tag{4.3.5-4}$$

$$\text{Let } u = \frac{\frac{xq}{1+x} - \mu_I}{\sigma_I}, \Rightarrow \frac{du}{dx} = \frac{q}{\sigma_I (1+x)^2} \tag{4.3.5-5}$$

$$\because \frac{\partial}{\partial x}[1 - Q(u)] = \frac{1}{\sqrt{2\pi}} \exp(\frac{-u^2}{2}) \cdot \frac{du}{dx} = \frac{1}{\sqrt{2\pi}} \exp(\frac{(\frac{xq}{1+x} - \mu_I)^2}{-2\sigma_I^2}) \cdot \frac{q}{\sigma_I (1+x)^2}$$

$$\Rightarrow f_X(x) = \frac{1}{\sqrt{2\pi}} \int_0^{\infty} \exp(\frac{(\frac{xq}{1+x} - \mu_I)^2}{-2\sigma_I^2}) \cdot \frac{q}{\sigma_I (1+x)^2} \cdot f_V(q) dq \tag{4.3.5-6}$$

(b) when $0 < x_k \le 1$, it implies $0 < I$

$$\begin{aligned} P[0 < X \le x_k] &= F_X(x_k) - F_X(0) = P[0 < I(1 - x_k) \le x_k \cdot |Q|] \\ &= P[0 < I \le \frac{x_k}{1 - x_k} |Q|] \\ &= \sum_{q_j} F_I(\frac{x_k \cdot q_j}{1 - x_k}) \cdot P[|Q| = q_j] - F_I(0) \end{aligned} \tag{4.3.5-7}$$

when $N \to \infty$,

$$F_X(x) - F_X(0) = \int_0^{\infty} F_I(\frac{xq}{1-x}) \cdot f_V(q) dq - F_I(0)$$

$$= \int_0^{\infty} [1 - Q(\frac{\frac{xq}{1-x} - \mu_I}{\sigma_I})] \cdot f_V(q) dq - [1 - Q(\frac{-\mu_I}{\sigma_I})]$$

$$= Q(\frac{-\mu_I}{\sigma_I}) - \int_0^{\infty} Q(\frac{\frac{xq}{1-x} - \mu_I}{\sigma_I}) \cdot f_V(q) dq \tag{4.3.5-8}$$

$$f_X(x) = \frac{d}{dx} F_X(x) = \int_0^{\infty} \frac{\partial}{\partial x}[1 - Q(\frac{\frac{xq}{1-x} - \mu_I}{\sigma_I})] \cdot f_V(q) dq \tag{4.3.5-9}$$

$$\text{Let } v = \frac{\frac{xq}{1-x} - \mu_I}{\sigma_I}, \quad \Rightarrow \frac{dv}{dx} = \frac{q}{\sigma_I (1-x)^2} \tag{4.3.5-10}$$

$$\because \ \frac{\partial}{\partial x}[1 - Q(v)] = \frac{1}{\sqrt{2\pi}} \exp(\frac{-v^2}{2}) \cdot \frac{dv}{dx} = \frac{1}{\sqrt{2\pi}} \exp(\frac{(\frac{xq}{1-x} - \mu_I)^2}{-2\sigma_I^2}) \cdot \frac{q}{\sigma_I (1-x)^2}$$

$$\Rightarrow f_X(x) = \frac{1}{\sqrt{2\pi}} \int_0^\infty \exp(\frac{(\frac{xq}{1-x} - \mu_I)^2}{-2\sigma_I^2}) \cdot \frac{q}{\sigma_I (1-x)^2} \cdot f_V(q) dq \tag{4.3.5-11}$$

In order to verify the above results, the derivation conditioned on I is provided in the next section. Note that the following derivation can be used with Eq.(4.3.5-6) and Eq. (4.3.5-11) to enhance the simulation results.

2). Derivation conditioned on I

(a) when $-1 \le x_k < 0$, it implies $I < 0$

$$F_X(x_k) = P[X \le x_k] = P[I(1+x_k) \le x_k \cdot |Q|] = P[|Q| \le \frac{1+x_k}{x_k} \cdot I]$$

$$= P[Q \le \frac{1+x_k}{x_k} \cdot I] - P[Q < \frac{1+x_k}{-x_k} \cdot I]$$

$$= \sum_{i_j=-1}^{0} F_Q(\frac{(1+x_k)\cdot i_j}{x_k}) \cdot P[I = i_j] - \sum_{i_j=-1}^{0} F_Q(\frac{(1+x_k)\cdot i_j}{-x_k}) \cdot P[I = i_j] \qquad (4.3.5\text{-}12)$$

when $N \to \infty$,

$$F_X(x) = \int_{-\infty}^{0} F_Q(\frac{(1+x)i}{x}) \cdot f_I(i)di - \int_{-\infty}^{0} F_Q(\frac{(1+x)i}{-x}) \cdot f_I(i)di$$

$$= \int_{-\infty}^{0} [1 - Q(\frac{\frac{(1+x)i}{x} - \mu_Q}{\sigma_Q})] \cdot f_I(i)di - \int_{-\infty}^{0} [1 - Q(\frac{\frac{(1+x)i}{-x} - \mu_Q}{\sigma_Q})] \cdot f_I(i)di$$

$$= -\int_{-\infty}^{0} Q(\frac{\frac{(1+x)i}{x} - \mu_Q}{\sigma_Q}) \cdot f_I(i)di + \int_{-\infty}^{0} Q(\frac{\frac{(1+x)i}{-x} - \mu_Q}{\sigma_Q}) \cdot f_I(i)di \qquad (4.3.5\text{-}13)$$

where, $f_I(i) = \frac{1}{\sqrt{2\pi\sigma_I^2}} \cdot \exp(\frac{-(i-\mu_I)^2}{2\sigma_I^2})$

$$f_X(x) = \frac{d}{dx} F_X(x)$$

$$= -\int_{-\infty}^{0} \frac{\partial}{\partial x} Q(\frac{\frac{(1+x)i}{x} - \mu_Q}{\sigma_Q}) \cdot f_I(i)di + \int_{-\infty}^{0} \frac{\partial}{\partial x} Q(\frac{\frac{(1+x)i}{-x} - \mu_Q}{\sigma_Q}) \cdot f_I(i)di \qquad (4.3.5\text{-}14)$$

Let $u_1 = \frac{\frac{(1+x)i}{x} - \mu_Q}{\sigma_Q}$, $\Rightarrow \frac{du_1}{dx} = \frac{-i}{\sigma_Q x^2}$ (4.3.5-15)

$$u_2 = \frac{\frac{(1+x)i}{-x} - \mu_Q}{\sigma_Q}, \quad \Rightarrow \frac{du_2}{dx} = \frac{i}{\sigma_Q x^2} \tag{4.3.5-16}$$

$$\because \quad \frac{\partial}{\partial x} Q(u) = \frac{-1}{\sqrt{2\pi}} \exp(\frac{-u^2}{2}) \cdot \frac{du}{dx}$$

$$\Rightarrow f_X(x)$$

$$= \frac{-1}{\sqrt{2\pi}} \int_{-\infty}^{0} \exp(\frac{(\frac{(1+x)i}{x} - \mu_Q)^2}{-2\sigma_Q^2}) \cdot \frac{i}{\sigma_Q x^2} \cdot f_I(i) di$$

$$+ \frac{-1}{\sqrt{2\pi}} \int_{-\infty}^{0} \exp(\frac{(\frac{(1+x)i}{x} + \mu_Q)^2}{-2\sigma_Q^2}) \cdot \frac{i}{\sigma_Q x^2} \cdot f_I(i) di$$

$$= \frac{-1}{\sqrt{2\pi}} \int_{-\infty}^{0} [\exp(\frac{(\frac{(1+x)i}{x} - \mu_Q)^2}{-2\sigma_Q^2}) + \exp(\frac{(\frac{(1+x)i}{x} + \mu_Q)^2}{-2\sigma_Q^2})] \cdot \frac{i}{\sigma_Q x^2} \cdot f_I(i) di \tag{4.3.5-17}$$

(b) when $0 < x_k \le 1$, it implies $0 < I$

$$F_X(x_k) = P[I(1-x_k) \le x_k \cdot |Q|] = P[|Q| \ge \frac{(1-x_k)}{x_k} \cdot I]$$

$$= P[Q \ge \frac{(1-x_k)}{x_k} \cdot I] + P[Q \le \frac{(1-x_k)}{-x_k} \cdot I]$$

$$= 1 - P[Q < \frac{(1-x_k)}{x_k} \cdot I] + P[Q \le \frac{(1-x_k)}{-x_k} \cdot I]$$

$$= 1 - \sum_{i_j=0}^{1} F_Q(\frac{(1-x_k) \cdot i_j}{x_k}) \cdot P[I = i_j] + \sum_{i_j=0}^{1} F_Q(\frac{(1-x_k) \cdot i_j}{-x_k}) \cdot P[I = i_j] \tag{4.3.5-18}$$

when $N \to \infty$,

$$F_X(x) = 1 - \int_0^\infty F_Q(\frac{(1-x)i}{x}) \cdot f_I(i)di + \int_0^\infty F_Q(\frac{(1-x)i}{-x}) \cdot f_I(i)di$$

$$= 1 - \int_0^\infty [1 - Q(\frac{\frac{(1-x)i}{x} - \mu_Q}{\sigma_Q})] \cdot f_I(i)di + \int_0^\infty [1 - Q(\frac{\frac{(1-x)i}{-x} - \mu_Q}{\sigma_Q})] \cdot f_I(i)di$$

$$= 1 + \int_0^\infty Q(\frac{\frac{(1-x)i}{x} - \mu_Q}{\sigma_Q}) \cdot f_I(i)di - \int_0^\infty Q(\frac{\frac{(1-x)i}{-x} - \mu_Q}{\sigma_Q})] \cdot f_I(i)di \qquad (4.3.5\text{-}19)$$

$$f_X(x) = \frac{d}{dx} F_X(x)$$

$$= \int_0^\infty \frac{\partial}{\partial x} Q(\frac{\frac{(1-x)i}{x} - \mu_Q}{\sigma_Q}) \cdot f_I(i)di - \int_0^\infty \frac{\partial}{\partial x} Q(\frac{\frac{(1-x)i}{-x} - \mu_Q}{\sigma_Q})] \cdot f_I(i)di \qquad (4.3.5\text{-}20)$$

Let $u_3 = \dfrac{\frac{(1-x)i}{x} - \mu_Q}{\sigma_Q}, \Rightarrow \dfrac{du_3}{dx} = \dfrac{-i}{\sigma_Q x^2}$ (4.3.5-21)

$$u_4 = \frac{\frac{(1-x)i}{-x} - \mu_Q}{\sigma_Q}, \Rightarrow \frac{du_4}{dx} = \frac{i}{\sigma_Q x^2} \qquad (4.3.5\text{-}22)$$

$$\because \quad \frac{\partial}{\partial x} Q(u) = \frac{-1}{\sqrt{2\pi}} \exp(\frac{-u^2}{2}) \cdot \frac{du}{dx}$$

$$\Rightarrow f_X(x) = \frac{1}{\sqrt{2\pi}} \int_0^\infty \exp(\frac{(\frac{(1-x)i}{x} - \mu_Q)^2}{-2\sigma_Q^2}) \cdot \frac{i}{\sigma_Q x^2} \cdot f_I(i)di$$

$$+ \frac{1}{\sqrt{2\pi}} \int_0^\infty \exp(\frac{(\frac{(1-x)i}{x} + \mu_Q)^2}{-2\sigma_Q^2}) \cdot \frac{i}{\sigma_Q x^2} \cdot f_I(i)di$$

$$= \frac{1}{\sqrt{2\pi}} \int_0^\infty [\exp(\frac{(\frac{(1-x)i}{x} - \mu_Q)^2}{-2\sigma_Q^2}) + \exp(\frac{(\frac{(1-x)i}{x} + \mu_Q)^2}{-2\sigma_Q^2})] \cdot \frac{i}{\sigma_Q x^2} \cdot f_I(i)di \qquad (4.3.5\text{-}23)$$

3).Summary of the CDF, pdf, mean and variance of $\frac{I}{|I|+|Q|}$

(a) CDF and pdf :

(i) for $-1 \le x \le 0$:

The CDF is given by

$$F_X(x) = 1 - \int_0^{\infty} Q(\frac{\frac{xq}{1+x} - \mu_I}{\sigma_I}) \cdot f_V(q)dq \qquad (4.3.5\text{-}24)$$

As for the pdf, it can be expressed in two forms as follow:

$$f_X(x) = \frac{1}{\sqrt{2\pi}} \int_0^{\infty} \exp(\frac{(\frac{xq}{1+x} - \mu_I)^2}{-2\sigma_I^2}) \cdot \frac{q}{\sigma_I (1+x)^2} \cdot f_V(q)dq \qquad (4.3.5\text{-}25)$$

or

$$f_X(x) = \frac{-1}{\sqrt{2\pi}} \int_{-\infty}^{0} [\exp(\frac{(\frac{(1+x)i}{x} - \mu_Q)^2}{-2\sigma_Q^2}) + \exp(\frac{(\frac{(1+x)i}{x} + \mu_Q)^2}{-2\sigma_Q^2})] \cdot \frac{i}{\sigma_Q x^2} \cdot f_I(i)di \qquad (4.3.5\text{-}26)$$

(ii) for $0 < x \le 1$:

The CDF is given by:

$$F_X(x) = 1 - \int_0^{\infty} Q(\frac{\frac{xq}{1-x} - \mu_I}{\sigma_I}) \cdot f_V(q)dq \qquad (4.3.5\text{-}27)$$

As for the pdf, it can be expressed in two forms as follow:

$$f_X(x) = \frac{1}{\sqrt{2\pi}} \int_0^{\infty} \exp(\frac{(\frac{xq}{1-x} - \mu_I)^2}{-2\sigma_I^2}) \cdot \frac{q}{\sigma_I (1-x)^2} \cdot f_V(q)dq \qquad (4.3.5\text{-}28)$$

or

$$f_X(x) = \frac{1}{\sqrt{2\pi}} \int_0^{\infty} [\exp(\frac{(\frac{(1-x)i}{x} - \mu_Q)^2}{-2\sigma_Q^2}) + \exp(\frac{(\frac{(1-x)i}{x} + \mu_Q)^2}{-2\sigma_Q^2})] \cdot \frac{i}{\sigma_Q x^2} \cdot f_I(i)di \qquad (4.3.5\text{-}29)$$

where, $f_V(q) = \frac{\sqrt{2}}{\sqrt{\pi\sigma_Q^2}} \exp(-\frac{q^2+\mu_Q^2}{2\sigma_Q^2}) \cdot \cosh(\frac{q\mu_Q}{\sigma_Q^2})$

$$f_I(i) = \frac{1}{\sqrt{2\pi\sigma_I^2}} \cdot \exp(\frac{-(i-\mu_I)^2}{2\sigma_I^2}) \qquad (4.3.5\text{-}30)$$

Note that the pdf expressed by Eq.(4.3.5-25) should be same as Eq.(4.3.5-26), and so are Eq.(4.3.5-28) and Eq.(4.3.5-29). Also note that there is one singularity point with Eq.(4.3.5-25), Eq.(4.3.5-26), Eq.(4.3.5-28) and Eq.(4.3.5-29) at $x=-1$, $x=0$, $x=+1$ and $x=0$, respectively. Those singularity points are shown as in Figure 4.3-1, Figure 4.3-2 and Figure 4.3-3.

In order to avoid the singularity effect, in our pdf simulation, we use Eq.(4.3.5-25) and Eq.(4.3.5-28) when $x \in [-0.5,0.5]$, and use Eq.(4.3.5-26) and Eq.(4.3.5-29) for remained data range of x.

It can also be proved that Eq.(4.3.5-25) is same as Eq.(4.3.5-26) as follow.

From Eq.(4.3.5-25), Eq.(4.3.4-2) and Eq.(4.3.4-4), we have

$$f_X(x) = \frac{1}{2\pi\sigma_Q} \int_0^{\infty} \exp(\frac{(\frac{xq}{1+x}-\mu_I)^2}{-2\sigma_I^2}) \cdot \frac{q}{\sigma_I(1+x)^2} \cdot [\exp(\frac{(q-\mu_Q)^2}{-2\sigma_Q^2}) + \exp(\frac{(q+\mu_Q)^2}{-2\sigma_Q^2})]dq \qquad (4.3.5\text{-}31)$$

Let $u = \frac{xq}{1+x}$, $\Rightarrow du = \frac{x}{1+x}dq$, and $q = \frac{(1+x)u}{x}$, then we have

$$f_X(x) = \frac{1}{2\pi\sigma_Q} \int_0^{-\infty} \exp(\frac{(u-\mu_I)^2}{-2\sigma_I^2}) \cdot \frac{u}{\sigma_I x(1+x)} \cdot [\exp(\frac{(\frac{(1+x)u}{x}-\mu_Q)^2}{-2\sigma_Q^2})$$

$$+ \exp(\frac{(\frac{(1+x)u}{x}+\mu_Q)^2}{-2\sigma_Q^2})] \cdot \frac{1+x}{x}du$$

$$= \frac{-1}{2\pi\sigma_I} \int_{-\infty}^{0} [\exp(\frac{(\frac{(1+x)u}{x}-\mu_Q)^2}{-2\sigma_Q^2}) + \exp(\frac{(\frac{(1+x)u}{x}+\mu_Q)^2}{-2\sigma_Q^2})] \cdot \frac{u}{\sigma_Q x^2} \cdot$$

$$\exp(\frac{(u-\mu_I)^2}{-2\sigma_I^2})]du$$

$$= \frac{-1}{\sqrt{2\pi}} \int_{-\infty}^{0} [\exp(\frac{(\frac{(1+x)u}{x} - \mu_Q)^2}{-2\sigma_Q^2}) + \exp(\frac{(\frac{(1+x)u}{x} + \mu_Q)^2}{-2\sigma_Q^2})] \cdot \frac{u}{\sigma_Q x^2} \cdot$$

$$[\frac{1}{\sqrt{2\pi\sigma_I^2}} \cdot \exp(\frac{(u-\mu_I)^2}{-2\sigma_I^2})] du$$

$$= \frac{-1}{\sqrt{2\pi}} \int_{-\infty}^{0} [\exp(\frac{(\frac{(1+x)u}{x} - \mu_Q)^2}{-2\sigma_Q^2}) + \exp(\frac{(\frac{(1+x)u}{x} + \mu_Q)^2}{-2\sigma_Q^2})] \cdot \frac{u}{\sigma_Q x^2} \cdot f_I(u) du$$

(4.3.5-32)

Note that Eq.(4.3.5-32) is indeed the same as Eq.(4.3.5-26).

Similarly, it can also be proved that Eq.(4.3.5-28) and Eq.(4.3.5-29) are same as follow.

From Eq.(4.3.5-28), Eq.(4.3.4-2) and Eq.(4.3.4-4), we have

$$f_X(x) = \frac{1}{2\pi\sigma_Q} \int_0^{\infty} \exp(\frac{(\frac{xq}{1-x} - \mu_I)^2}{-2\sigma_I^2}) \cdot \frac{q}{\sigma_I (1-x)^2} \cdot [\exp(\frac{(q-\mu_Q)^2}{-2\sigma_Q^2}) + \exp(\frac{(q+\mu_Q)^2}{-2\sigma_Q^2})] dq$$

(4.3.5-33)

Let $u = \frac{xq}{1-x}$, $\Rightarrow du = \frac{x}{1-x} dq$, and $q = \frac{(1-x)u}{x}$, then we have

$$f_X(x) = \frac{1}{2\pi\sigma_Q} \int_0^{\infty} \exp(\frac{(u-\mu_I)^2}{-2\sigma_I^2}) \cdot \frac{u}{\sigma_I x(1-x)} \cdot [\exp(\frac{(\frac{(1-x)u}{x} - \mu_Q)^2}{-2\sigma_Q^2})$$

$$+ \exp(\frac{(\frac{(1-x)u}{x} + \mu_Q)^2}{-2\sigma_Q^2})] \cdot \frac{1-x}{x} du$$

$$= \frac{1}{2\pi\sigma_I} \int_0^{\infty} [\exp(\frac{(\frac{(1-x)u}{x} - \mu_Q)^2}{-2\sigma_Q^2}) + \exp(\frac{(\frac{(1-x)u}{x} + \mu_Q)^2}{-2\sigma_Q^2})] \cdot \frac{u}{\sigma_Q x^2} \cdot$$

$$\exp(\frac{(u-\mu_I)^2}{-2\sigma_I^2})] du$$

$$= \frac{1}{\sqrt{2\pi}} \int_0^{\infty} [\exp(\frac{(\frac{(1-x)u}{x} - \mu_Q)^2}{-2\sigma_Q^2}) + \exp(\frac{(\frac{(1-x)u}{x} + \mu_Q)^2}{-2\sigma_Q^2})] \cdot \frac{u}{\sigma_Q x^2} \cdot$$

$$[\frac{1}{\sqrt{2\pi\sigma_I^2}}\cdot\exp(\frac{(u-\mu_I)^2}{-2\sigma_I^2})]du$$

$$=\frac{1}{\sqrt{2\pi}}\int_0^\infty[\exp(\frac{(\frac{(1-x)u}{x}-\mu_Q)^2}{-2\sigma_Q^2})+\exp(\frac{(\frac{(1-x)u}{x}+\mu_Q)^2}{-2\sigma_Q^2})]\cdot\frac{u}{\sigma_Q x^2}\cdot f_I(u)du \tag{4.3.5-34}$$

Note that Eq.(4.3.5-34) is indeed the same as Eq.(4.3.5-29).

(b) Mean:

$$\mu_X = E[X]=\int_{-1}^{1}x\cdot f_X(x)dx$$

$$=\int_{-1}^{1}xdF_X(x)=x\cdot F_X(x)\Big|_{-1}^{1}-\int_{-1}^{1}F(x)dx=1-\int_{-1}^{1}F(x)dx \tag{4.3.5-35}$$

(c) Variance:

$$\sigma_X^2 = E[X^2]-\mu_X^2=\int_{-1}^{1}x^2\cdot f_X(x)dx-\mu_X^2$$

$$=x^2\cdot F_X(x)\Big|_{-1}^{1}-\int_{-1}^{1}2F(x)\cdot xdx-\mu_X^2$$

$$=1-2\int_{-1}^{1}x\cdot F(x)dx-[1-\int_{-1}^{1}F(x)dx]^2$$

$$=-2\int_{-1}^{1}x\cdot F(x)dx+2\int_{-1}^{1}F(x)dx-(\int_{-1}^{1}F(x)dx)^2 \tag{4.3.5-36}$$

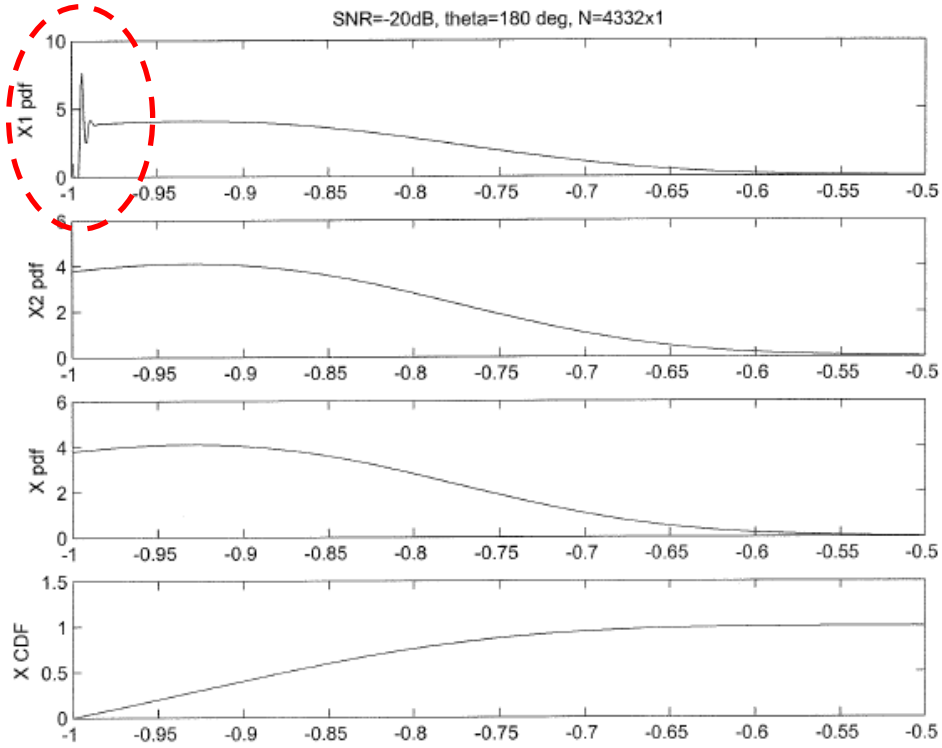

Figure 4.3-1: X1 pdf, Eq.(4.3.5-25), shows a singularity point at x=-1

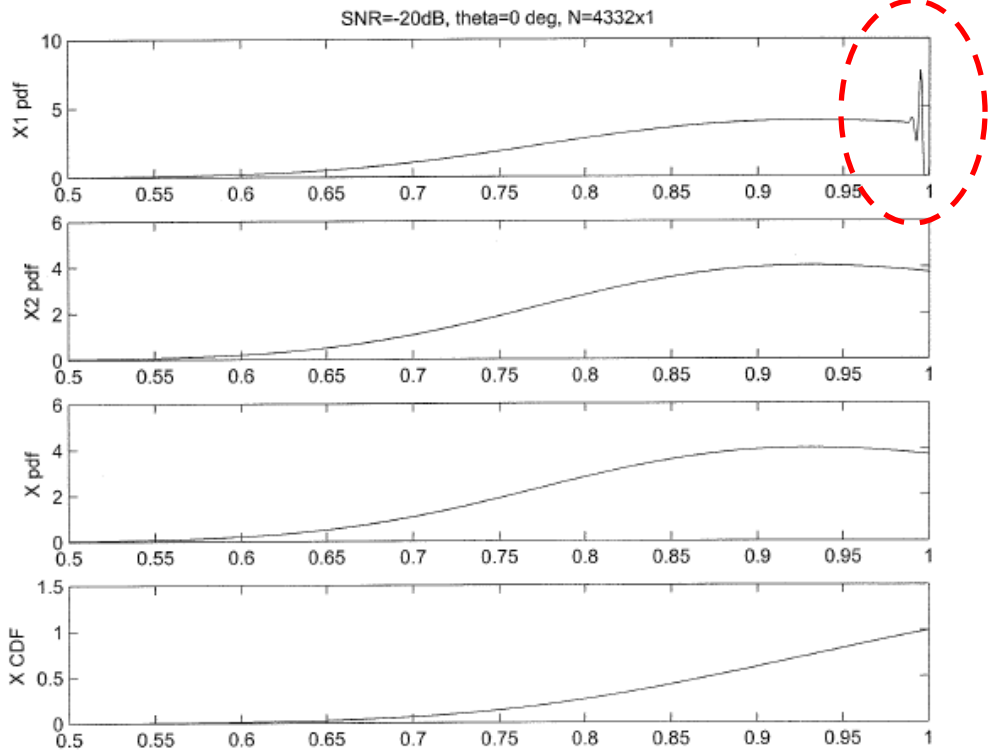

Figure 4.3-2: X1 pdf, Eq.(4.3.5-28), shows a singularity point at x=1

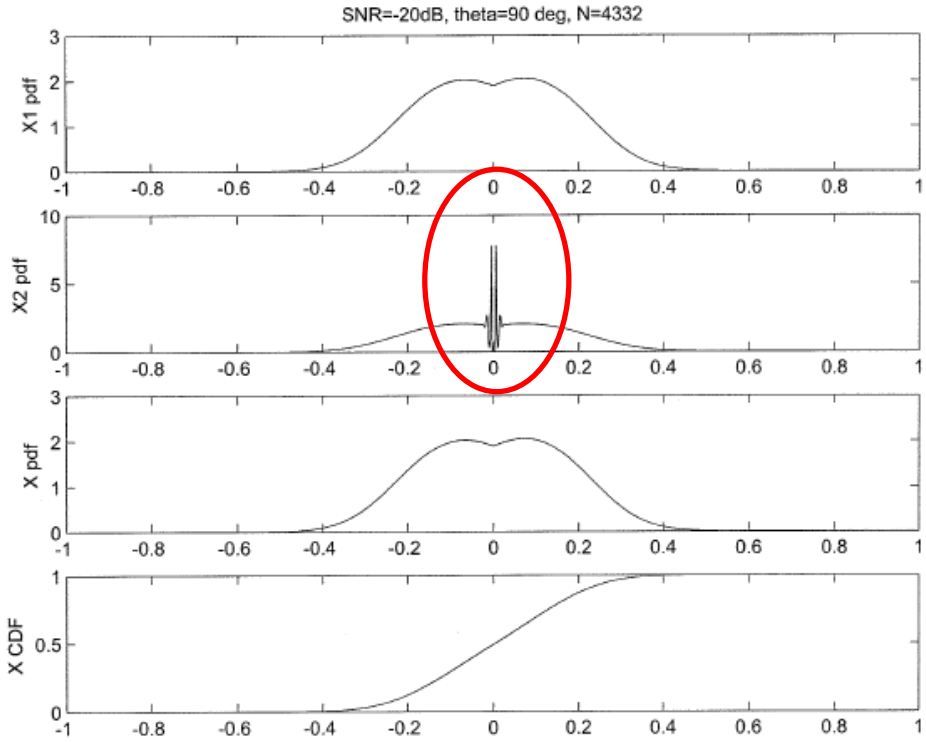

Figure 4.3-3: X2 pdf, Eq.(4.3.5-26) and Eq.(4.3.5-29), shows a singularity point at x=0

5. Simulation and Experimental Results

5.1 Discriminator Simulation

The probability-density-function of X, i.e., $\frac{I}{|I|+|Q|}$, derived in section 4.3, depends on SNR and phase. A series of simulation are performed to verify the analytical results when SNR=-10dB, -20dB, -30dB where GNSS applications usually fall in the range between. In addition, various cases of θ=17°, 73°, 90° are considered. Note that it's sufficient to perform the simulation over $\theta \in [0^\circ, 90^\circ]$, since it is symetric about $\theta = 90^\circ$.

Figure 5.1-1(a), 5.1-1(b), and 5.1-1(c) show the histograms and the analytical results when SNR= -30 dB and various θ angles. Figure 5.1-2(a), 5.1-2(b), and 5.1-2(c) show the histograms and the analytical results when SNR= -20 dB and various θ angles. Finally, Figure 5.1-3(a), 5.1-3(b), and 5.1-3(c) show the histograms and the analytical results when SNR= -10 dB and various θ angles.

From all the simulation results as shown in Figure 5.1-1, Figure 5.1-2 and Figure 5.1-3, we see that the Monte Carlo simulation results are fully consistent with the analytical results no matter what the SNR is.

The analytical results of mean and variance of X with respect to θ when SNR= -20dB, -30dB, and -10dB are plotted in Figure 5.1-4, Figure 5.1-5, and Figure 5.1-6 respectively. The phase estimate, $\hat{\theta}$, and estimate error calculated based on mean of X are also plotted in these figures for reference.

From Figure 5.1-4(a) and Figure 5.1-4(b), it shows that the variance and the estimate error reduce as the number of samples increases. When the number of sample, N, is 17328, the maximum variance is 0.008 and the mzximum estimate error is around 7°. However, when the number of samples increases to 4 times, i.e., N = 69312, then the maximum variance and estimate error reduce to 0.0025 and 4.1° respectively.

From Figure 5.1-4, Figure 5.1-5 and Figure 5.1-6, it shows that the variance reduces as the SNR increases. When N=69312, and SNR= -30dB, -20dB, and -10dB, the maximum variances are 0.019, 0.0024, and 0.00034 respectively.

As for the maximum estimate error, we note that it always occurs at θ = 17°, 73°, 108°, 163° by 4.1° for SNR=-20dB and -10dB.

1). Histogram of simulated results and calculated pdf when SNR=-30 dB

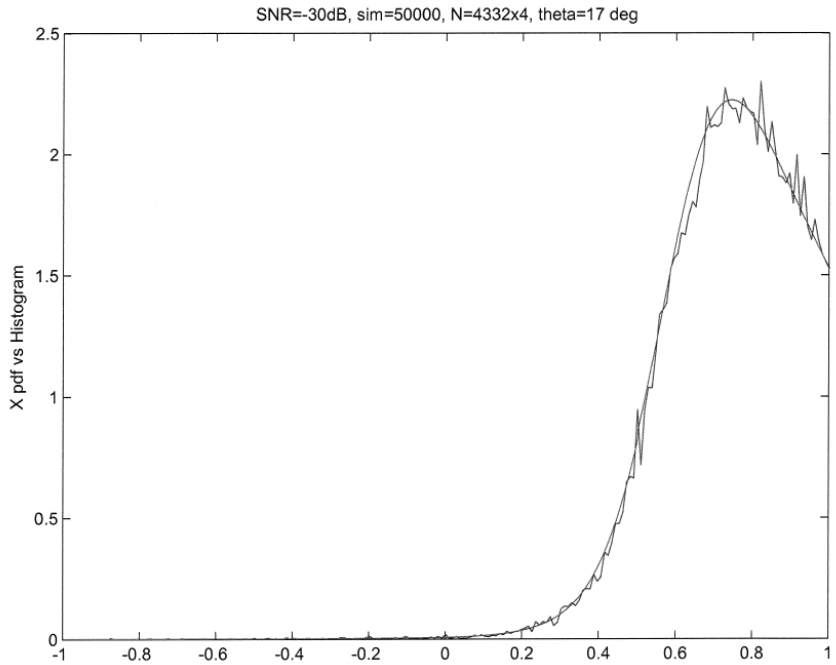

Figure 5.1-1(a):Histogram (blue) and pdf(red), when SNR=-30dB, θ=17°

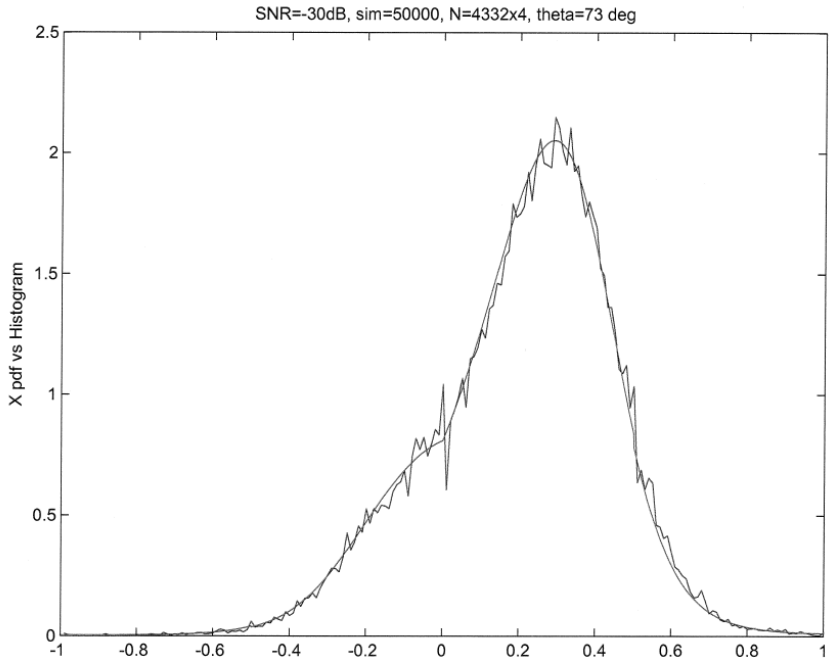

Figure 5.1-1(b): Histogram (blue) and pdf (red), when SNR=-30dB, θ=73°

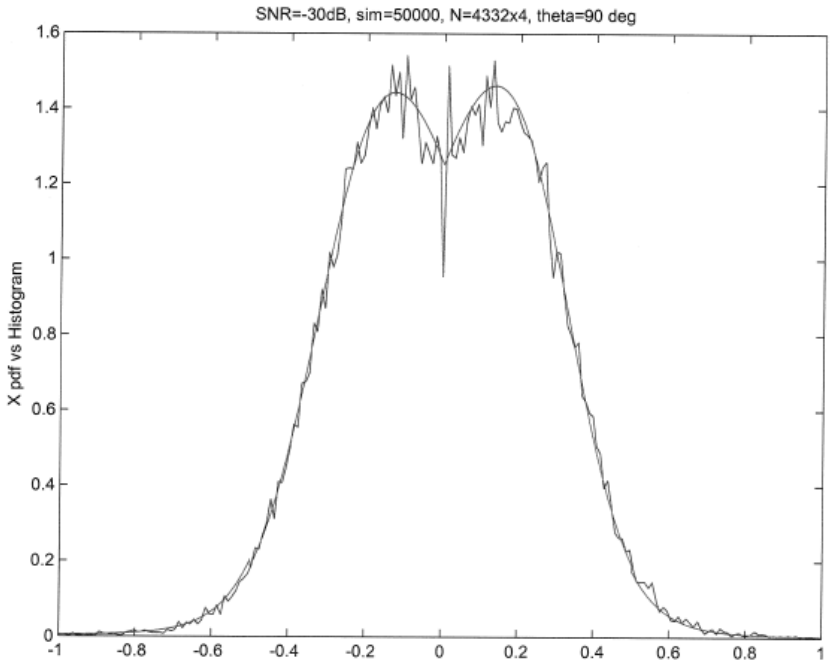

Figure 5.1-1(c):Histogram (blue) and pdf (red), when SNR=-30dB, θ=90°

2). Histogram of simulated results and calculated pdf when SNR=-20dB

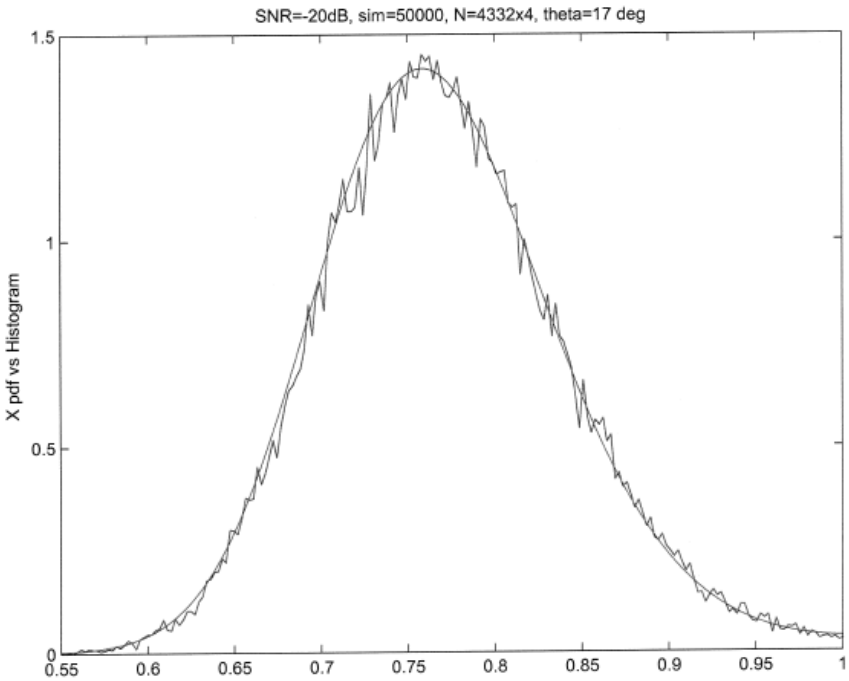

Figure 5.1-2(a): Histogram (blue) and pdf(red), when SNR=-20dB, θ=17°

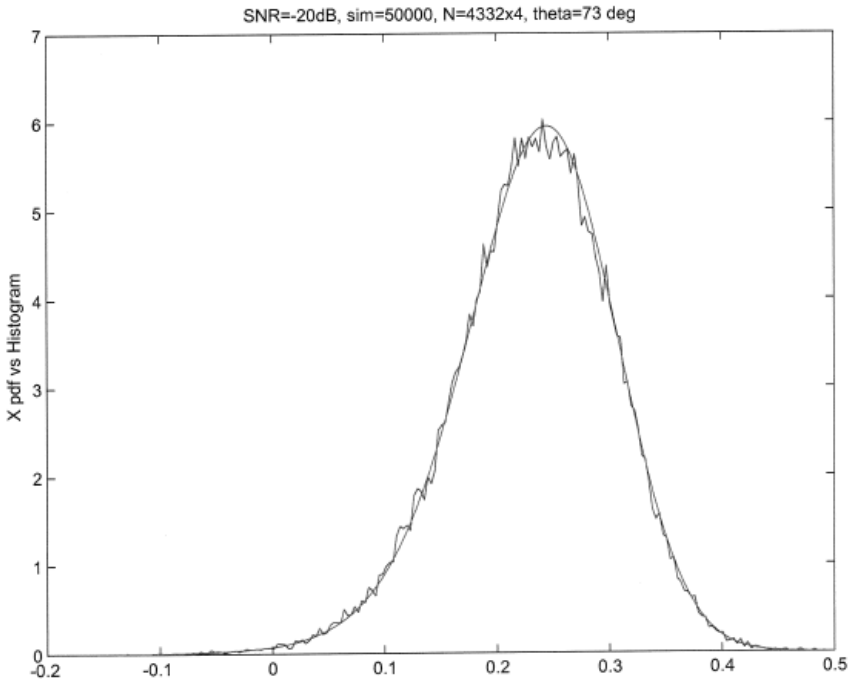

Figure 5.1-2(b): Histogram (blue) and pdf (red), when SNR=-20dB, θ=73°

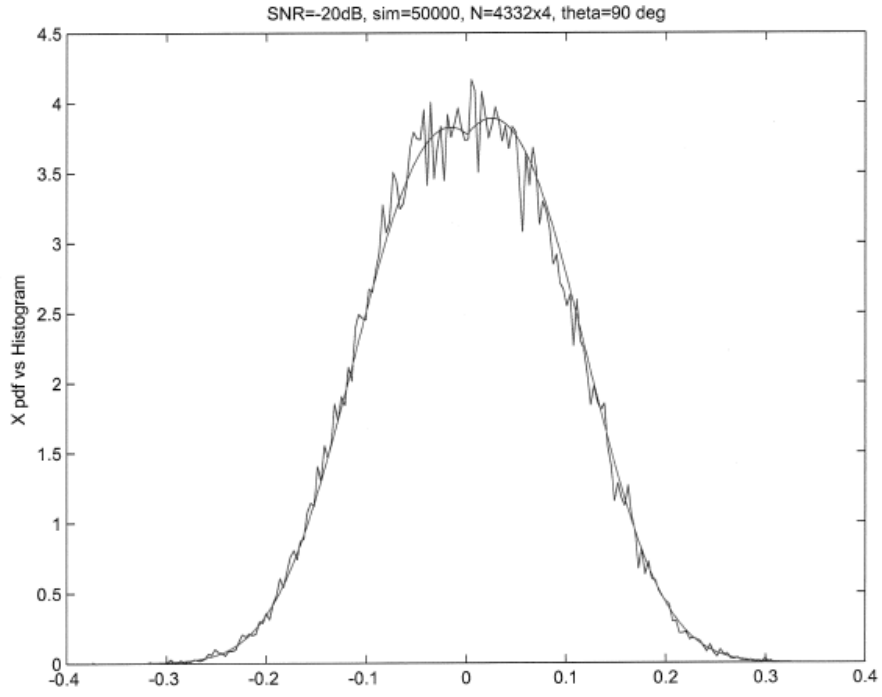

Figure 5.1-2(c): Histogram (blue) and pdf (red), when SNR=-20dB, θ=90°

3). Histogram of simulated results and calculated pdf when SNR= -10 dB

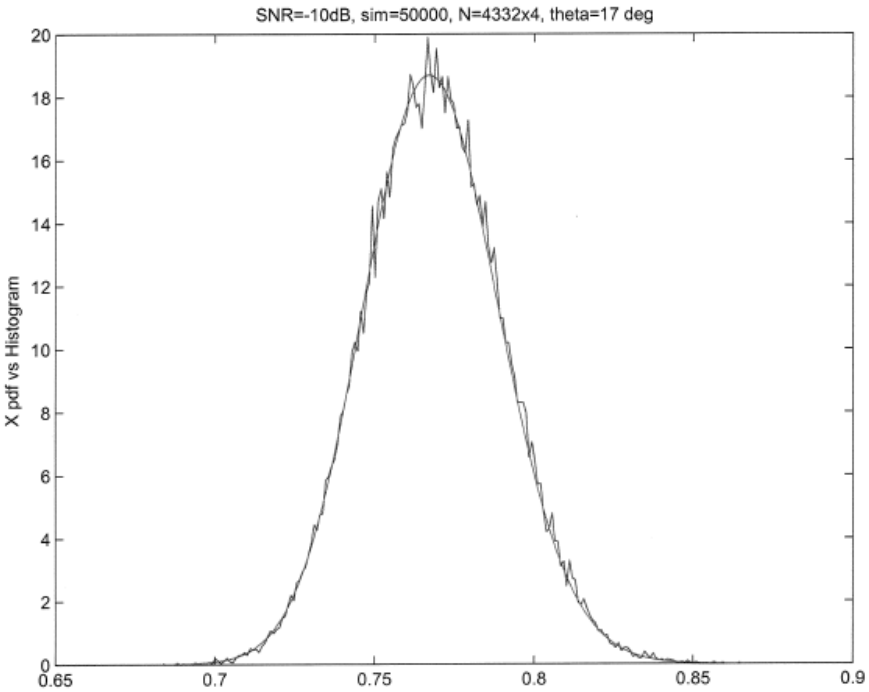

Figure 5.1-3(a): Histogram (blue) and pdf (red), when SNR=-10dB, θ=17°

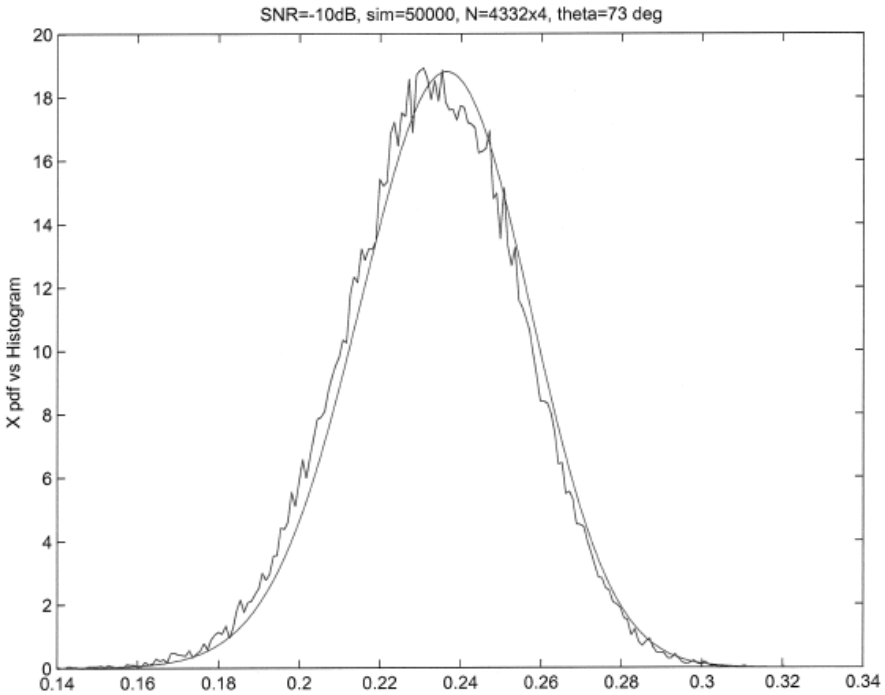

Figure 5.1-3(b): Histogram (blue) and pdf (red), when SNR=-10dB, θ=73°

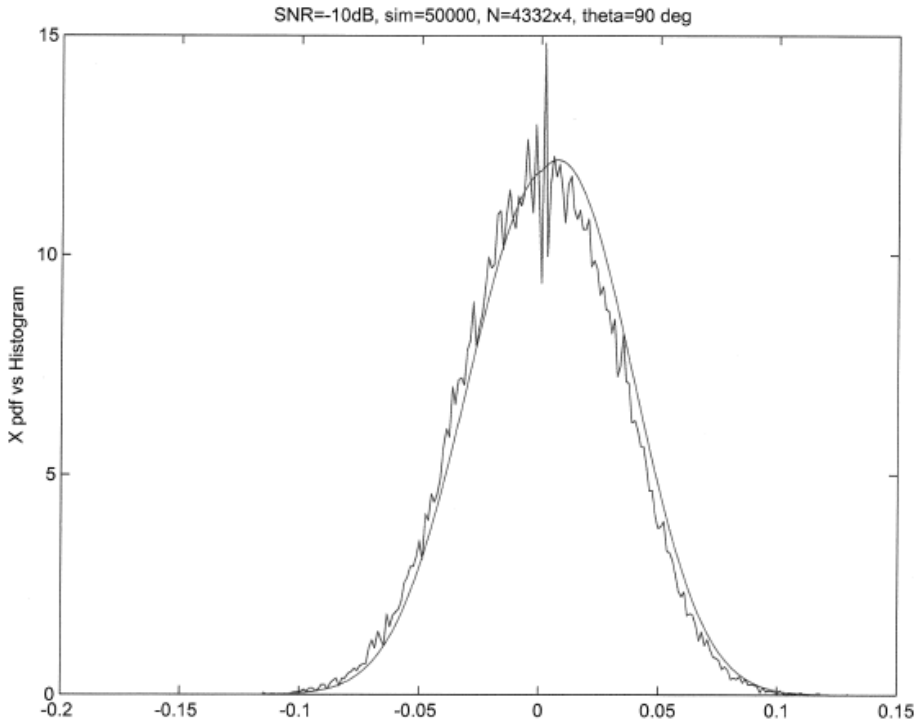

Figure 5.1-3(c): Histogram (blue solid) and pdf(red dashed),when SNR=-10dB, θ=90°

4). Mean, variance, phase estimate, and estimation error when SNR= -20 dB

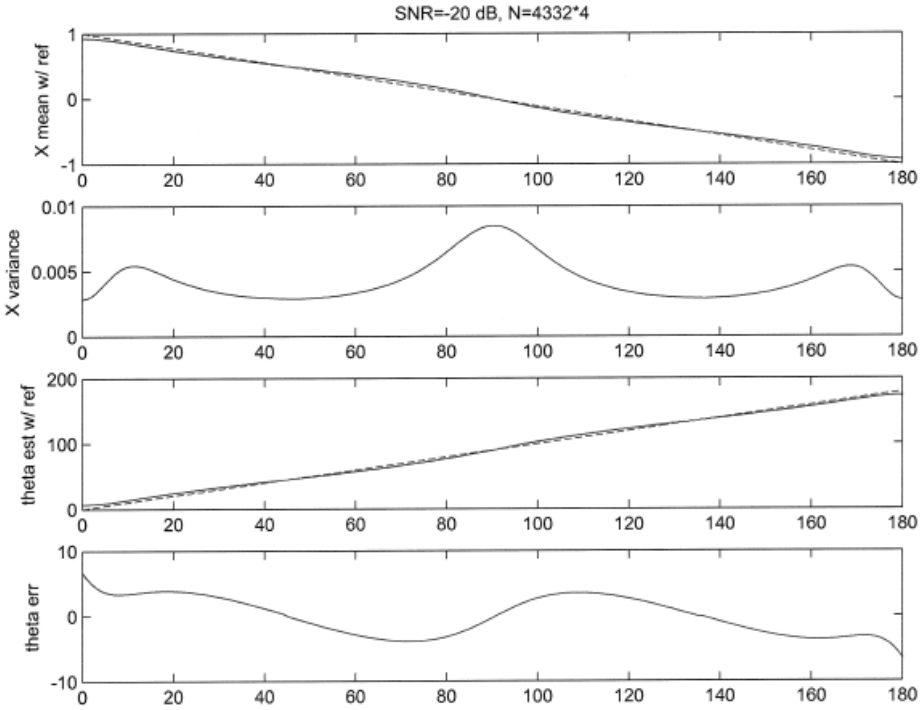

Figure 5.1-4(a):Mean with a reference line(red dashed), variance, $\hat{\theta}$ with a reference line(red dashed), estimation error of $\hat{\theta}$ when SNR=-20dB, N=4332*4

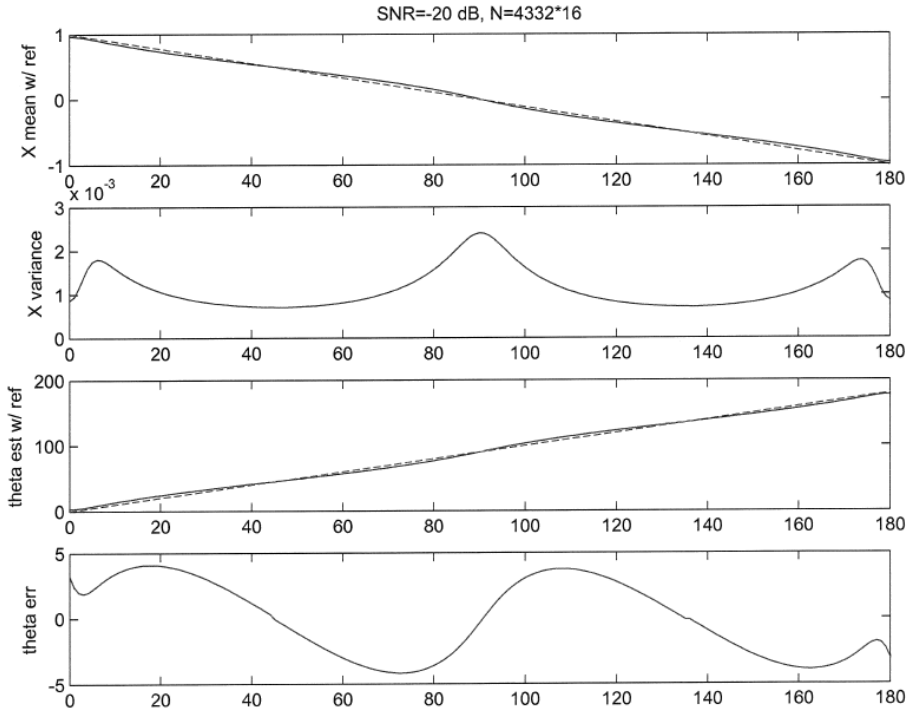

Figure 5.1-4 (b): Mean with a reference line(red dashed), variance, $\hat{\theta}$ with a reference line(red dashed), estimation error of $\hat{\theta}$ when SNR=-20dB, N=4332*16

5). Mean, variance, phase estimate, and estimation error when SNR= -30dB and -10dB

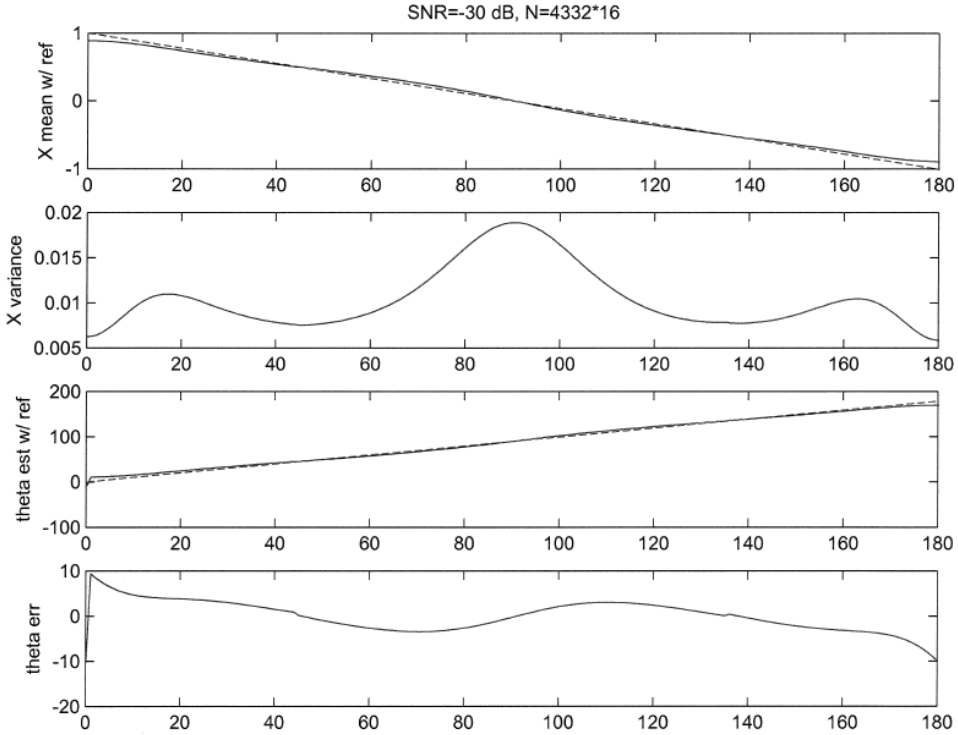

Figure 5.1-5: Mean with a reference line(red dashed), variance, $\hat{\theta}$ with a reference line(red dashed), estimation error of $\hat{\theta}$ when SNR=-30dB, N=4332*16

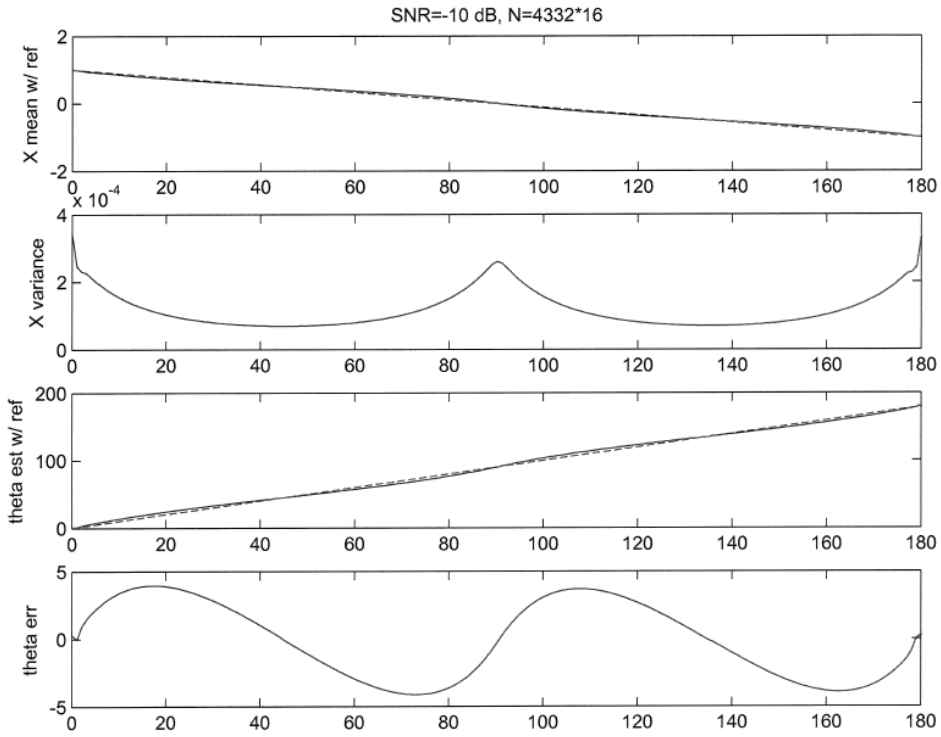

Figure 5.1-6: Mean with a reference line(red dashed), variance, $\hat{\theta}$ with a reference line(red dashed), estimation error of $\hat{\theta}$ when SNR=-10dB, N=4332*16

5.2 Tracking loop experiment

The SGR consists of a RF front end of Signal Tap and self-developed PC-based software using C programming for acquisition, pull-in and tracking. The received signal is sampled at 4.096 MHz with 1-bit ADC. The phase discriminator used is the NB-DPD.

5.2.1 Receiver at static mode

The data used is true GPS data received by an antenna located at a fixed position with WGS84 latitude, longitude, and height of 24°47', 121°21' and 300 m, respectively. The date is March 6th, 2007 and the starting GPS time is 180304 sec. The time length of the data is 90 seconds. Using the proposed structure, we can successfully track PRN 4, 17, 20 and 28, and extract the ephemeras data and obtain the user position. The tracking quality is illustrated by a clip of the inphase and quadrature correlator outputs for PRN 27 as shown in Figure 5.2-1.

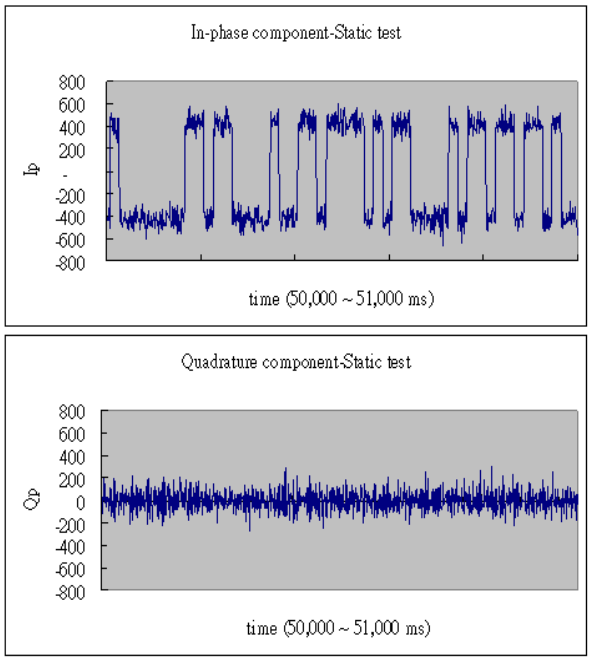

Figure 5.2-1 Inphase and quadrature correlator output for PRN 27 in static mode

A comparison of the in-phase correlator outputs when the discriminators NB-DPD and APD are used in static mode is shown in Figure 5.2-2. Note that the GPS signal is typically lower than noise floor by 19 dB. For such a low SNR case, from Figure 5.2-2, the in-phase correlator output of NB-DPD is almost same as APD.

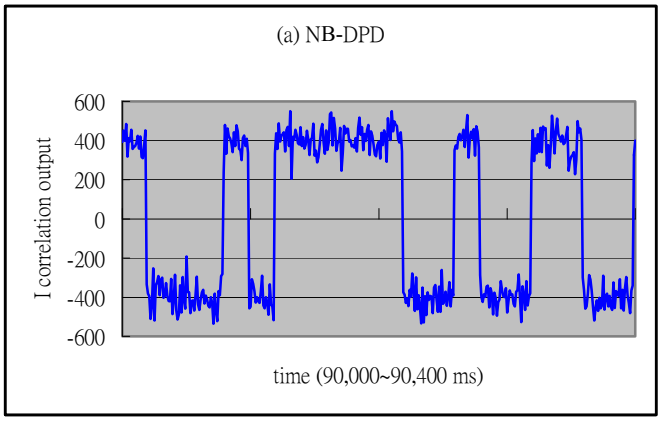

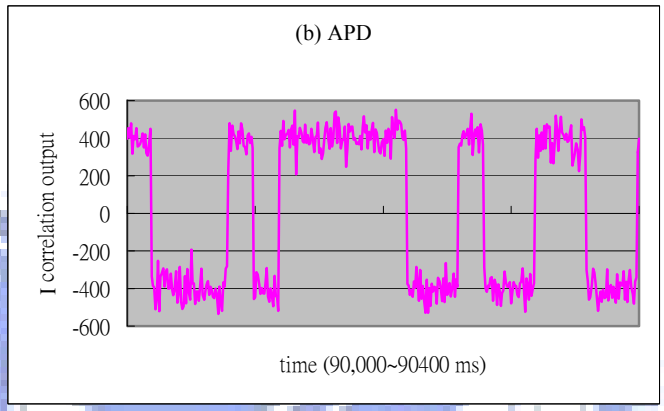

Figure 5.2-2 Inphase correlator outputs for NB-DPD and APD in static mode

5.2.2 Receiver at dynamic mode

The data used is simulated data generated by SPIRENT GSS7700 GPS/SBAS simulator. The simulation date is August 9th, 2002 and the starting GPS time is 475363 sec. The simulated spacecraft is initially at the position with WGS84 latitude, longitude, and height of 7°32', 130°51' and 352197 m, respectively. From the result, the proposed structure can successfully track PRN 's with the relative acceleration 13.33 m/sec^2 (about 1.36g) as shown in Figure 5.2-3.

A comparison of the in-phase correlator outputs and the estimated frequency when the discriminators NB-DPD and APD are used in dynamic mode are shown in Figure 5.2-4 and Figure 5.2-5 respectively. Again, for such a low SNR case, the in-phase correlator outputs and the estimated frequencies are almost of the same.

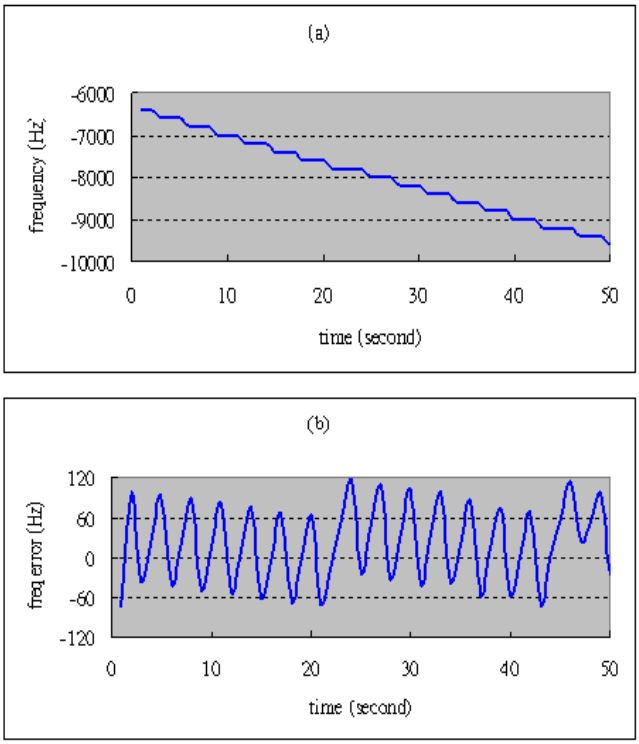

Figure 5.2-3 (a) Estimated Doppler frequency in FLL and (b) estimated frequency error

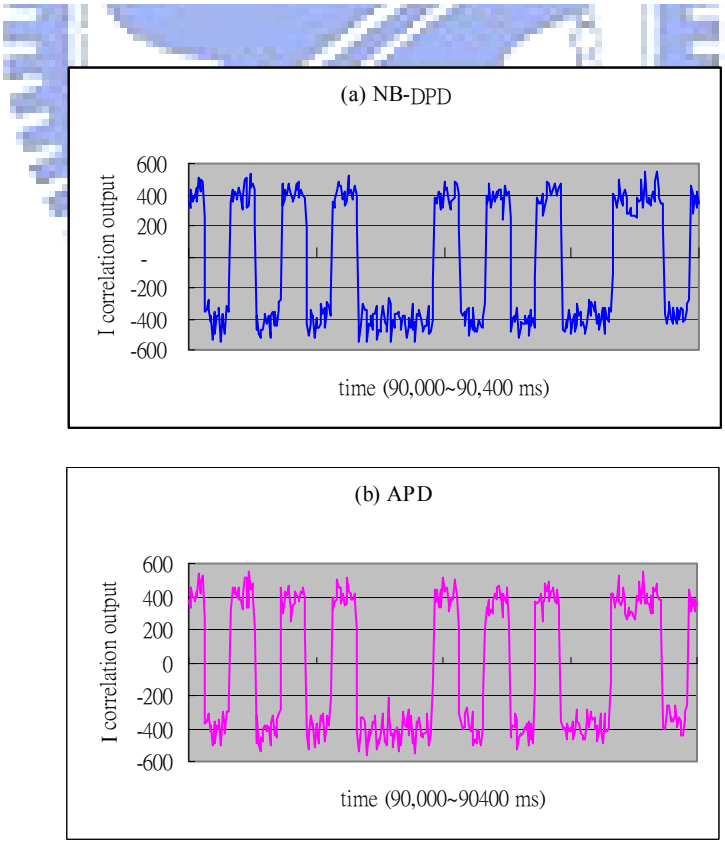

Figure 5.2-4 Inphase correlator outputs for NB-DPD and APD in dynamic mode

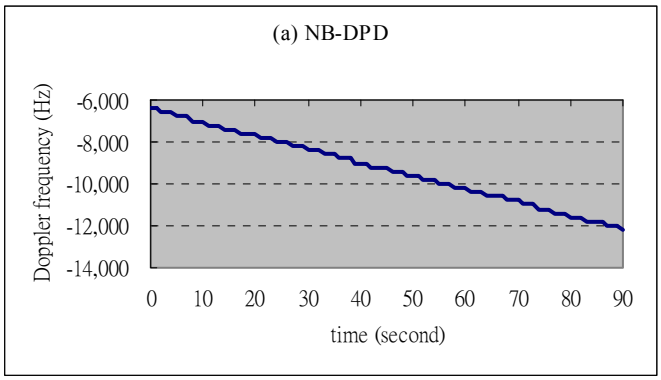

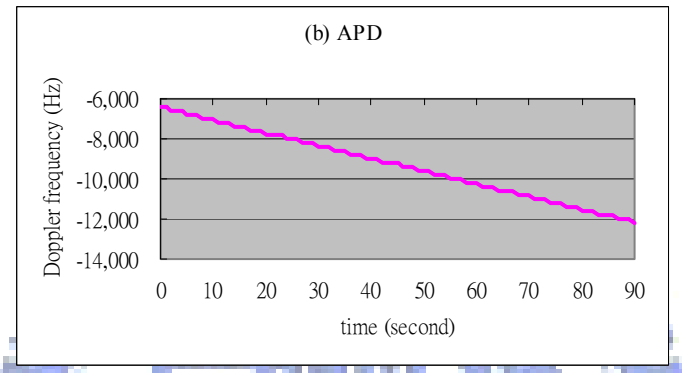

Figure 5.2-5 Estimated frequencies for NB-DPD and APD in dynamic mode.

6 Conclusion

The significant feature of the PCPC structure is the improvement of correlator output magnitude because it prevents the quantization effect on carrier phase ambiguity. The improvement becomes more critical significant when very few bits ADC are used. The proposed PCPC structure is implemented in 1-bit SGR and successfully track PRN's both in static mode and dynamic mode. Regarding the implementation of the FLL, it's worth to mention that the phase offset effect of local carrier table must be considered in order to attain correct fequency variation. The effect is induced because the beginning phase of a pre-established carrier table is always zero while the local carrier of the following interval may have a nonzero beginning phase.

The proposed NB-DPD is developed based on digital approach which intuitively derives the carrier phase difference using the time delay between received signal and local reference signal. The derivations of the probability properties of the NB-DPD estimator are provided as in section 4.3. A series of simulation are performed to verify the analytical results when SNR= -10dB, -20dB, and -30dB with various phase-angle cases. The analytical results are indeed verified by computer simulation as in section 5.1.

From the simulation results, the Monte Carlo simulation results are consistent with the analytical results no matter what the SNR is. Note that the variance and the estimate error reduce as the number of samples increases. For the SNR= -20dB case, when the number of sample, N, is 17328, the maximum variance is 0.008 and the mzximum estimate error is around 7°. When the number of samples increases to 4 times, i.e., N = 69312, then the maximum variance and estimate error reduce to 0.0025 and 4.1° respectively. It's also noted that the variance reduces as the SNR increases. When N=69312, and SNR= -30dB, -20dB, and -10dB, the maximum variances are 0.019, 0.0024, and 0.00034 respectively. As for the maximum estimate error, we note that it always occurs at $\theta = 17°, 73°, 108°, 163°$ by 4.1° for SNR above -20dB.

The NB-DPD is based on binary symmetrical probability model considering both noiseless ($P_{01} = P_{10} = 0$) and noisy environments. It is equivalent to DPD in noiseless case and thus inherits high accuracy properties of DPD in high SNR cases. The NB-DPD performs generally better than the DPD in noisy cases. The lower the SNR is,

the greater the improvement. Moreover, the NB-DPD works almost as well as arctangent-phase discriminator (APD) in low SNR environments and thus can be applied to GNSS receivers.

The NB-DPD is implemented in a one-bit software-defined GPS receiver using PCPC structure. The experimental results demonstrate the feasibility of the proposed scheme. It is worth to mention that PCPC structure can be applied to phase discriminators whose range is between $-\pi$ and π (compared with arctangent $-\pi/2 \sim \pi/2$). Hence NB-DPD works well in PCPC structure.

The SGR, whose tracking loop is implemented with the PCPC structure and the NB-DPD discriminator, is tested in receiving both the real GPS signals and the simulated high-dynamic GPS signals as shown in section 5.2. From the experiment results, the SGR can successfully track four satellite signals with good tracking quality, and extract the ephemeras data and obtain user position.

As we consider high dynamic environments, e.g., LEO satellite with altitude 350 km, the maximum Doppler shift and Doppler rate induced by a L1 carrier emitted from a GPS satellite are 46 kHz and 90 Hz/sec, respectively.[26] From our experimental results, the SGR remains tracking when Doppler shift and Doppler rate achieve 42.6kHz and 643 Hz/sec (12.5g), respectively. Note that this verified capability is limited by the current available data and the greater tolerance is expected when the associated data is available in the future. Hence our algorithm and structure can be well applied in SGR for high dynamic environments.

From the comparison of the in-phase correlator outputs and the estimated frequency when the discriminator NB-DPD and APD are used in both static and dynamic modes as shown in Figure 5.2-2, Figure 5.2-4, and Figure 5.2-5. It's noted that the SGR tracking performance as implemented with NB-DPD is almost same as with APD using less computation.

Finally, the progress of modern digital technology and the efficient computations of NB-DPD make it very attractive in real-time digital processing receivers.

Bibliography

[1] C.-F. Chang and M.-S. Kao, ”High-Accuracy Carrier Phase Discriminator for One-Bit Quantized Software-Defined Receivers”, IEEE Signal Processing Letter, vol. 15, pp.397-400, 2008.

[2] B. Parkinson and J. Spilker, Global Positioning System: Theory and Applications, AIAA, Volume I, 1996.

[3] E. Kaplan and C. Hegarty, Understanding GPS Principles and Applications, 2nd edition, Artech, 2006

[4] James B-Y Tsui, Fundamentals of Global Positioning System Receivers, John Wiley & Sons, 2000

[5] H. Chang, "Presampling Filtering, Sampling and Quantization Effects on the Digital Matched Filter Performance", Proceedings of International Telemetering Conference, San Diego, CA, pp. 889-915, Sep. 1982.

[6] 2008 Gibbons Media & Research LLC

[7] S. C. Gupta, “Phase-locked Loops”, Proceedings of IEEE, vol. 63, pp.291-306, Feb. 1975.

[8] F. M. Gardner, Phase Lock Techniques, 2nd edition, New York: Wiley, 1979.

[9] John G. Proakis, Digital Communication, 4th edition, McGraw Hill, 2001

[10] M. S. Grewal, L. R. Weill and A. P. Andrews, “Global Positioning Systems, Inertial Navigation, and Integration”, John Wiley & Sons, 2001.

[11] C.-F. Chang, R.-M. Yang and M.-S. Kao, “1-Bit High Accuracy Carrier Phase Discriminator” under review of IEEE Transactions on Signal Processing.

[12] P.Ward, J.W. Betz and C.J. Hegarty, “Satellite Signal Acquisition, Tracking and Data Demodulation”, in Understanding GPS: Principles and Applications, Second Edition, E.D. Kaplan and C.J. Hegarty, Artech House, Norwood, MA, 2006.

[13] Marvin K. Simon, “Probability Distributions Involving Gaussian Random Variables”, 2002 Kluwer Academic Publishers

[14] K. Krumvieda, “A Complete IF Software GPS Receiver: A Tutorial About the Details”, Proceedings of ION GPS 2001.

[15] C. Lachapelle and M. Cannon, “Implementation of a Software GPS Receiver”, Proceedings of ION GNSS Sep. 2004.

[16] R. Vaughan, N. Scott, D. White, “The Theory of Bandpass Sampling”, IEEE Trans. on Signal Processing, vol. 39, no. 9, pp. 1973-1984, 1991.

[17] D. Akos, M. Stockmaster, J. Tsui and J. Caschera, “Direct Bandpass Sampling of Multiple Distinct RF Signals”, IEEE Trans. on Communications, vol. 47, no. 7, pp. 983-988, 1999.

[18] W. C. Lindsey and C.-M. Chie, “A Survey of Digital Phase-Locked Loops”, Proceedings of IEEE, vol. 69, no. 4, pp.410-431, 1981.

[19] A. Brown and B. Wolt, ”Digital L-Band Receiver Architecture with Direct RF Sampling”, IEEE Position Location and Navigation Symposium, pp. 209–216, April 1994.

[20] T. C. Marek, ”Performance of ASCAMP DPSK Downlink Processor”, Proceedings of MILCOM ’94, pp. 519–523, 1994.

[21] P. H. Wu, ”The Optimal BPSK Demodulator with a 1-bit A/D Front-end”, Proceedings of MILCOM ’98, pp. 730–735, 1998.

[22] B. Ledvina and M. Psiaki etc ”A Real-Time GPS Civilian L1/L2 Software Receiver,” Proceedings of ION GNSS 2004, pp. 986–1005, September 2004.

[23] K. Borre, D. Akos, N. Bertelsen, P. Rinder and S. Jensen, A Software-defined GPS and Galileo Receiver, Birkhauser, 2007.

[24] C.-F. Chang, R.-M. Yang, M.-S. Kao and J.-C. Juang, ”A Novel Scheme and Modi fied Structures for Improved Software GPS Receiver ”, Proceedings of ION GNSS September,2007,

[25] C.-F. Chang, R.-M. Yang and M.-S. Kao, "Phase Discriminating Device and Method", applied US patent under review.

[26] Hao-Wen Cheng, Yu T. Su, "GPS Signal Acquisitions in High Dynamic Environments", Thesis 1996.